

1 Developing a tile drainage module for the Cold Regions

2 Hydrological Model: Lessons from a farm in Southern

3 Ontario, Canada

4

5 Mazda Kompanizare*^{&#}, Diogo Costa⁺, Merrin L. Macrae[&], John W. Pomeroy^{*}, Richard M. Petrone[&]

6 ^{*}Centre for Hydrology, University of Saskatchewan, Canmore and Saskatoon, Canada

7 ⁺ Mediterranean Institute for Agriculture, Environment and Development, University of Évora, Mediterranean

8 Institute for Agriculture, Environment and Development, Portugal

9 [&]University of Waterloo, Waterloo, Canada

10 [#]Corresponding author: kompanizare.mazda@usask.ca

11

12 Abstract

13 Systematic tile drainage is used extensively in poorly drained agricultural lands to remove excess
14 water and improve crop growth; however, tiles can also transfer nutrients from farmlands to
15 downstream surface water bodies, leading to water quality problems. Thus, there is a need to
16 simulate the hydrological behaviour of tile drains to understand the impacts of climate or land
17 management change on agricultural surface and subsurface runoff. The Cold Regions
18 Hydrological Model (CRHM) is a physically based, modular modeling system developed for cold
19 regions. Here, a tile drainage module is developed for CRHM. A multi-variable, multi-criteria
20 model performance evaluation strategy was deployed to examine the ability of the module to
21 capture tile discharge under both winter and summer conditions (NSE>0.29, RSR<0.84 and PBias
22 <20 for tile flow and saturated storage water table simulations). Initial model simulations run at a

23 15-min interval did not satisfactorily represent tile discharge; however, model simulations
24 improved when the time step was lengthened to hourly but also with the explicit representation of
25 capillary rise for moisture interactions between the rooting zone and groundwater, demonstrating
26 the significance of capillary rise above the ~~saturated storage layer water table~~ in the hydrology of
27 tile drains in loam soils. Novel aspects of this module include the sub-daily time step, which is
28 ~~shorted-shorter~~ than most existing models, ~~and which may enable future water quality modules to~~
29 ~~be added~~, and the use of field capacity and its corresponding pressure head to provide estimates of
30 drainable water and the thickness of the capillary fringe, rather ~~using~~ than using detailed soil
31 retention curves that may not always be available. An additional novel aspect is the demonstration
32 that flows in some tile drain systems can be better represented and simulated when related to
33 shallow ~~saturated storage water table~~ dynamics.

34

35 Keywords: tile drainage, cold regions, hydrological model, capillary fringe, drainable water,
36 ~~saturated storage water table~~ fluctuations

37

38

39 **1. Introduction**

40

41 Harmful algal blooms and eutrophication in large freshwater lakes surrounded by agricultural
42 lands are major environmental challenges in Canada and globally. The transport of nutrients,
43 particularly phosphorus, in runoff from agricultural fields into ~~rivers, ponds and eventually~~
44 lakes surface water is an important contributor to the increased frequency of algal blooms being
45 experienced in North America and elsewhere (Sharpley et al., 1995; Correll, 1998; Filippelli, 2002;

46 Ruttenberg, 2005; Schindler, 2006; Quinton et al., 2010; Costa et al., 2022). Although nNutrient
47 transport from agricultural fields can occur via both surface runoff and tile drainage (Radcliffe et
48 al., 2015), ~~and~~ recent increases in the frequency and magnitude of algal blooms in Lake Erie in
49 North America have been attributed to tile drainage (King et al., 2015; Jarvie et al., 2017). Tile
50 drain systems lower the seasonally high waterhigh-water tables in poorly drained fields, reduce
51 the retention time of soil water, lessening ~~g~~ waterlogging in fields and improving both crop growth
52 and field trafficability for farmers (Cordeiro and Ranjan, 2012; Kokulan et al., 2019a). However,
53 they are also important pathways for dissolved nutrients and particulate ~~nutrients~~ material
54 (Kladivko et al., 1999; Tomer et al., ~~2015~~2003). In Alberta, tile drains have also been used to
55 address salinity issues (Broughton and Jutras, 2013). It has been estimated that 14% of farmlands
56 in Canada (ICID, 2018) and 45% of fields in Southern Ontario, Canada (ICID, 2018; Kokulan,
57 2019) are drained by tile systems. ~~In Alberta, tile drains have also been used to address salinity~~
58 ~~issues (Broughton and Jutras, 2013).~~ Given their importance in hydrological budgets and
59 biogeochemical transport, there is a need to understand the controlling mechanisms of water and
60 nutrient export from tile systems as an integral part of the broader, modified hydrological system.
61 ~~The ability to integrate a dynamic quantification of tile drainage from fields in hydrological models~~
62 ~~can help understand the relative importance of this human-induced process as it interplays with an~~
63 ~~array of other phenomena, including energy and physical mass balance hydrological processes,~~
64 ~~climate change, and the impacts of modified land management practices on runoff and nutrient~~
65 ~~export.~~

66 There are several models that can represent tile drainage, controlled tile drainage and
67 surface runoff in different soil types at the small basin scale, which mainlytypically calculate the
68 amount of gravitational drainage from the soil, such as HYPE (Lindstrom et al., 2010; Arheimer

69 et al., 2015), DRAINMOD (Skaggs, 1978, 1980a; Skaggs et al., 2012), MIKE SHE (Refsgaard
70 and Storm, 1995) and SWAT (Arnold et al., 1998; Koch et al., 2013; Du et al., 2005; Du et al.,
71 2006; Green et al., 2006; Kiesel et al., 2010). These models include conceptual components for
72 many key hydrological processes, ~~andbut research shows that they~~ have been primarily designed
73 and tested for temperate regions (Costa et al., 2020a). In Canada and other cold regions, some
74 unique hydrological processes such as ~~frozen soil~~, snowmelt, rain on snow, and runoff over and
75 infiltration into frozen or partially-frozen soils may also be ~~very~~ important (Rahman et al., 2014;
76 Cordeiro et al., 2017; Pomeroy et al., 1998, 2007; Fang et al., 2010, 2013). Many hydrological
77 processes, such as the sublimation of snow, energy balance snowmelt, and infiltration into frozen
78 soils, are strongly affected by temperature and the phase changes of water, which make many
79 existing models developed for warm regions less appropriate for regions with cold seasons
80 (Pomeroy et al., 2007; ~~Pomeroy et al.~~, 2013; ~~Pomeroy et al.~~, 2016; Fang et al., 2010, 2013). Even
81 for temperate regions, the representation of cold season processes is often underrepresented in
82 models (Costa et al., 2020a).

83 Since the use of tile drainage is ~~becoming popular~~increasing in many cold regions ([Kokulan](#)
84 [et al., 2019a](#); [OMAFRA, 2023](#)), it has become important to integrate such human-induced
85 processes in the specialized hydrological modelling tools that have been developed for these
86 regions, such as the Cold Regions Hydrological Modelling platform (CRHM, Pomeroy et al., 2007;
87 2013; 2022). CRHM was initially developed in 1998 to assemble and explore the hydrological
88 understanding developed from a series of research basins spanning Canada and elsewhere into a
89 flexible, modular, object-oriented, multiphysics platform for simulating hydrological processes
90 and basin response in cold regions (Pomeroy et al., 2007; 2022). The modular CRHM platform

91 allows for multiple representations of forcing data interpolation and extrapolation, hydrological
92 model spatial and physical process structure and parameter values.

93 Many existing models typically operate at default daily or monthly time intervals, which
94 is inadequate for the prediction of many short-duration “flashy” hydraulic ~~responses events often~~
95 observed in tiles (Puer et al., 2020; Vivekananthan, 2019; Vivekananthan et al., 2019; Lam et al.,
96 2016a, 2016b; Macrae et al., 2019). Indeed, the ability to simulate shorter time intervals (e.g.,
97 hourly) facilitates the ability to capture both the rising and falling limbs of tile flow hydrographs,
98 as well as the magnitude of peak flows, both of which are important to tile drain chemistry and
99 export (Rozemeijer et al., 2016; Williams et al., 2015, 2016; Macrae et al., 2019).

100 ~~Hydrological process models such as DRAINMOD, MIKE SHE and SWAT use a~~
101 ~~combination of empirical and physically based formulations for the simulation of tile flow derived~~
102 ~~by Hooghoudt (1940), Kirkham (1957), van Schilfgaarde (1974), Bouwer and van Schilfgaarde~~
103 ~~(1963) and Skaggs et al., (1978). Such formulations contemplate both cases where the water table~~
104 ~~is below and above the ground surface (Kirkham, 1957). In contrast, simulations of tile drainage~~
105 ~~in other models such as HYPE use empirically derived recession curves (Eckersten et al., 1994) to~~
106 ~~simulate tile flow and soil hydrological storage (typically represented as water table). In cases~~
107 ~~where there is a need for more focus on soil matrix hydrology and less need for understanding~~
108 ~~hydrological processes at the catchment scale and the relative contribution of tiles (and its~~
109 ~~interplay), modellers tend to use specialised porous media PDE-based (partial differential~~
110 ~~equation based) numerical models such as HYDRUS (Simunek et al., 2011) and MACRO (Larsbo~~
111 ~~and Jarvis, 2003).~~

112 The amount of water transported by tiles depends on soil moisture dynamics, hydraulic
113 gradients and the positioning of the saturated storage layer~~water table~~, which are in turn affected

114 by many factors, including soil type, surface topography and morphology, as well as the local
115 climate and the hydrological characteristics of the field (Frey et al. 2016; Klaiber et al., 2020;
116 Coelho et al., 2012; King et al., 2015). Thus, to provide reliable estimations of water loss from
117 farmland via surface runoff and tile flow, models must be able to predict soil moisture and
118 saturated layer storage ~~and the water table elevation accurately~~ (Brockley, 1976; Rozemeijer et al.,
119 2016; Javani-Jouni et al., 2018). ~~Early Many Some~~ studies have shown that in some soil types,
120 including silty loam and clay loam soils, the drainable water is less than expected based on the
121 effective porosity (e.g., ~~Skeggs Skaggs~~ et al., 1978; Raats and Gardner, 1974). Raats and Gardner
122 (1974) have argued that the calculation of drainable porosity requires knowledge of water table
123 elevation and the distribution of soil moisture above the saturated storage layer ~~water table~~. Skaggs
124 et al. (1978) added that the calculation of drainable porosity should consider “the unsaturated zone
125 drained to equilibrium with the water table”. However, because the soil column is often composed
126 of different soil layers with varying physical characteristics, drainable porosity varies with
127 evapotranspiration rate, soil water dynamics and the depth of saturated water (Logsdon et al., 2010;
128 Moriasi et al., 2013). In a sandy loam soil, Lam et al. (2016a, 2016b) demonstrated that tile
129 drainage was not initiated until soil was at or above field capacity. Williams et al. (2019) observed
130 in the American Midwest that tile drainage was not initiated until the field storage capacity had
131 been exceeded. It has also been shown that despite the presence of tile drains, the soil above the
132 tile ~~may did~~ not always drain all the gravitational water following a rainfall/snowmelt event and
133 the soil may remain at or above field capacity (Skaggs et al., 1978; Lam et al., 2016a).
134 ~~Therefore This means that~~ , the soil drainable water content may be considerably smaller than the
135 storage capacity. This is related to matric potential within the vadose zone, which is driven by the
136 soil characteristics but can also be due to the development of a capillary fringe that reduces the

137 rate of vertical percolation through the unsaturated zone, reducing tile flow (Youngs, 2012).
138 Despite this evidence, some saturated flow models that simulate tile flow overlook the effect of
139 capillary rise and over-estimate the soil drainable water. Other models that represent unsaturated
140 flow (i.e., HYDRUS 3D, Simunek et al., 2011) using Richard’s Equation (Richards, 1931) capture
141 the effect of capillary rise and saturation-pressure variation within the soil profile and assess the
142 soil drainable water more accurately. Although the effect of capillary rise is considered in
143 DRAINMOD through the concept of drainable porosity (represented as a “water yield”) (Skaggs,
144 1980b), and is calculated for layered soil profiles (Badr,1978), it requires detailed information
145 surrounding the soil water characteristic curve (Skaggs, 1980b). Although it is indeed optimal to
146 use soil-specific water characteristic curves, [Twarakawi-Twarakavi](#) et al. (2009) found that it ~~was~~
147 is possible to employ average representative values from the soil water characteristic curve to
148 represent soil drainable water where ~~a soil-specific curves are was~~ not available, with some
149 reduction in. ~~and They they found in this case that the~~ model performance ~~was reduced~~.

150 In this study, a new Tile Drainage Module (TDM) was developed and incorporated within
151 the physically based, modular Cold Regions Hydrological Modelling (CRHM) platform (Pomeroy
152 et al., 2022) to enable hydrological simulations in tile-drained farm fields in cold agricultural
153 regions. As a first iteration, the new module was developed for a field with sloping ground and
154 loam soil with imperfect drainage. Such landscapes are common in the Great Lakes Region (e.g.,
155 Michigan and Vermont, USA and Ontario, Canada) and tile drainage in such landscapes has not
156 been as widely studied as it has been in clay-dominated soil. In this module, considerations were
157 explicitly included for the effects of capillary rise and annual fluctuations in saturated storage
158 ~~groundwater water table fluctuations~~ on drainable soil water storage. The use of field capacity and
159 groundwater/soil saturated storage ~~water elevation head~~ ([Twarakawi-Twarakavi](#) et al., 2009) to

160 modulate soil drainable water across the soil profile, including the capillary fringe region, is an
161 innovative aspect of the model that has been demonstrated to circumvent the need for water
162 characteristic curves. The development of this physically based module provides insight into
163 hydrological processes in tile drainage from sloping landscapes with imperfect drainage, which
164 are increasingly being artificially drained ([Cordeiro and Ranjan, 2012](#); [Kokulan et al., 2019a](#);
165 [OMAFRA, 2023](#)).

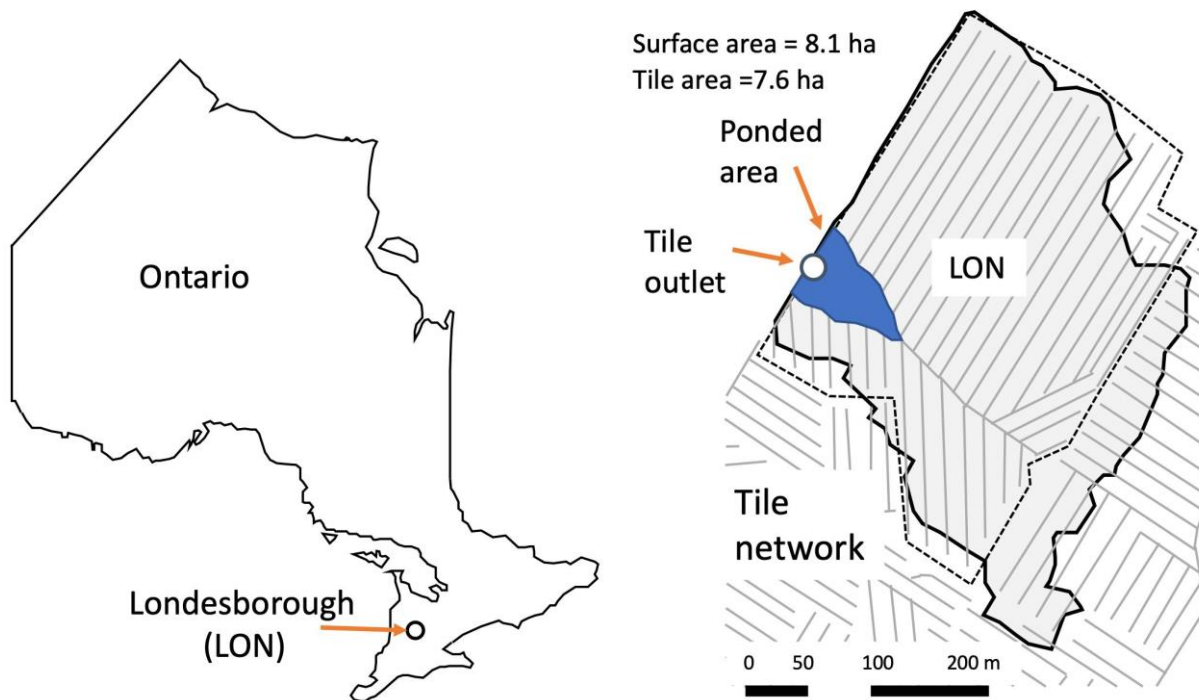
167 **2. Materials and Methods**

168 *2.1 Study area*

169 The study site is a ~10 ha farm field located near Londesborough, Ontario at UTM 17T 466689m
170 E, 4832203m N, shown as LON in Fig. 1a. Mean annual precipitation recorded in this region is
171 1247 mm (ECCC, 2020). Mean air temperature is 7.2 °C, with annual maxima in July (25.9 °C)
172 and minima in January (-10.2 °C), (ECCC, 2020). Soil [texture-type](#) has been identified as Perth
173 clay loam (Gr. Br. Luvisolic), with a slope between 0.2 and 3.5%. The field is systematically
174 drained with a tile depth of 0.9 m and a spacing of 14 m (laterals). The tile network collects
175 infiltrated water from about 75% of the field (~ 7.6 ha) but may also receive lateral groundwater
176 flow from neighbouring fields. Water yields from the tile drain laterals (10 cm diameter) are
177 discharged via a common tile outlet (main, 15 cm diameter) below ground. Surface runoff from
178 the field is directed toward a common outlet on the surface using plywood berms installed along
179 the field edge (see van Esbroeck et al., 2016). The tile and surface runoff outlets do not join into a
180 common outlet and are fully separated from one another, even during surface ponding events. The
181 field is a corn-soy-winter wheat rotation with cover drops and rotational conservation till (shallow
182 vertical tillage every three years). Additional details related to farming practices are provided in

183 Plach et al. (2019), soil characteristics are provided in Plach et al. (2018a) and Plach et al. (2018b)
184 and equipment and monitoring are provided in van Esbroeck et al., (2016). The outlets for both
185 surface and tile flow are located at the edge of the field and drain into an adjacent field (Fig. 1b).
186 Water tends to accumulate in a topographic low in the field, in front of the field outlet during
187 snowmelt or high-intensity rainfall events, presumably due to either surface runoff or return flow
188 (see ponded area, Fig. 1b). However, surface water or elevated soil moisture conditions are not
189 observed in this topographic low during smaller events or dry periods of the year, suggesting that
190 this saturated ponding is not in a perennial groundwater discharge zone. Although surface ponding
191 is observed in the topographic depression within the field, water discharges freely at the opposite
192 end of the culvert, facilitating the measurement of flow.

193



194

195 a)

b)

196 b) Figure 1. (a) Location of the study area in South of Ontario and the (b) Londesborough (LON) farm with its tile network.

197
198
199
200
201
202
203
204
205
206
207
208
209
210
211
212
213
214
215
216
217
218
219
220

2.2 CRHM: The modelling platform

CRHM is a modular hydrological process modelling platform that allows users to select relevant process submodules and apply them as needed to their study. For example, The modular the
CRHM platform includes options for empirical and physically based calculations of precipitation phase, snow redistribution by wind, snow interception, sublimation, sub-canopy radiation, snowmelt, infiltration into frozen and unfrozen soils, hillslope water movement, actual evapotranspiration, wetland fill and spill, soil water movement, groundwater flow and streamflow (Pomeroy et al., 2007; 2022). Where appropriate, it is able to calculates runoff from rainfall and snowmelt as generated by infiltration excess and/or saturated overland flow, flow over partially frozen soils, detention flow, shallow subsurface flow, preferential flow through macropores and groundwater flow (Pomeroy et al., 2007; 2022). ~~Water quality nNutrients losses in water can also be simulated in CRHM (Costa et al., 2021), although this was not done in the current study.~~
Modules of a CRHM model can be customized to basin setup, such as delineating and discretizing the basin, conditioning observations for extrapolation and interpolation in the basin, or are process-support algorithms such as for estimating longwave radiation, complex terrain wind flow, or albedo dynamics, but most modules ~~commonly~~ address hydrological processes such as evapotranspiration, infiltration, snowmelt, and streamflow discharge. CRHM discretizes basins into hydrological response units (HRU) for mass and energy balance calculations, each with unique process representations, parameters, and position along flow pathways in the basin. HRU are connected by blowing snow, surface, subsurface and groundwater flow and together generate streamflow which is routed to the basin outlet. The size of ~~TDM~~ HRUs is flexible and can be as small as the size of a single tile pipe (e.g., 1 m) times the pipe spacing (which was 14 m in our

221 case study region), and as large as entire tile networks within a given farm or study area. CRHM
222 does not require a stream within a modelled basin. The feature allows CRHM to model the
223 hydrology of cold regions dominated by storage and episodic runoff, such as agricultural fields.

224 Although CRHM has the capability to represent many hydrological and thermodynamic
225 processes, not all processes need/must be represented in all situations. The modular design of the
226 CRHM platform enables the user to activate or ~~inactive-inactivate~~ specific processes to optimize
227 the model for a particular situation. This is a modelling approach that enables testing different
228 modelling hypotheses and has been pioneered by CRHM and other models, which has inspired a
229 range of hydrological (e.g., SUMMA, Clark et al., 2015a, 2015b), hydrodynamic (e.g., mizuRoute,
230 Mizukami et al., ~~2015~~2016) and biogeochemical (e.g., OpenWQ, Costa et al., 2023a, ~~2023b~~)
231 modelling tools. For example, in the current study, blowing snow was not employed in CRHM as
232 it does not appear to be significant at the study site (periodic snow surveys showed relatively
233 uniform snow cover). ~~Similarly, P~~preferential flow into tile drains was not ~~included in developed~~
234 ~~for~~ the current simulation. ~~as a~~ Although ~~it it can be is~~ a key process in ~~some~~ clay loam soils,
235 ~~previous studies at the study site have shown that it is not as it does not appear to be a significant the~~
236 ~~case here~~ driver of preferential flow into tile drains ~~at the study site~~, which is a combination of clay-
237 ~~loam and silt-loam soils in coarse textured soil~~ (Pleur et al., 2020; Macrae et al., 2019), ~~and was~~
238 ~~consequently it was not included in our model at this stage. We used h~~Hydrograph analysis
239 ~~(Macrae et al., 2019) and conservative tracer (electrical conductivity and major ions, as well as~~
240 ~~temperature) over multiple years (Pleur et al., 2020) showed that and found minimal~~ preferential
241 ~~flow was minimal at this site as well as other similar sites. For this reason, preferential flow was~~
242 ~~not included in this study. However, we will certainly continue exploring this transport mechanism~~
243 ~~in future studies. We did not model preferential flow in this study, and it will be assessed in future~~

244 ~~studies.~~ Freeze-thaw of soil can occur in the study region, leading to partially frozen soils.
245 However, the extent of freezing ~~varies and differ~~ with snowpack development, winter temperatures
246 and ~~other radiation~~ ~~tive factors~~. Data collected over an 8-year period at this site found soil freezing
247 was restricted to brief periods and such freezing never extended below 10 cm depth (Macrae,
248 unpublished data) ~~which is insufficient for soils to behave as frozen ground for infiltration~~
249 ~~calculations~~. Consequently, freeze-thaw processes were ~~also not~~ deployed in the CRHM model of
250 ~~this site employed in the current study. As the model is improved further in the future, these and~~
251 ~~other model simplifications should be addressed~~ ~~uch processes can be included in future studies to~~
252 ~~further develop the model.~~ Freeze-thaw processes in soil were also not employed here as there is
253 very little seasonal soil frost in the temperate Great Lakes region due to the persistent snow cover,
254 and where soil frost occurs, it is restricted to brief periods and shallow depths (above 10 cm depth)
255 (Macrae unpublished data).

256

257 2.3 Observations and input data for the model

258 Tile flow, water table elevation (~~saturated storage~~ ~~water table~~ elevation head) and surface flow
259 were measured at the site between Oct. 2011 and Sept. 2018 at 15-minute intervals. It was not
260 possible to install more than one measuring station for water table elevation and soil moisture at
261 the site due to farming activity; consequently, water table elevation head and soil moisture were
262 measured at the approximate midpoint of the field at the edge-of-field. Both tile flow rates and
263 surface runoff were determined using simultaneous measurements of flow velocity and water
264 depths in each of the pipes at the edge-of-field using Hach Flo-tote sensors and an FL900 data
265 logger- (Onset Ltd.) (Table A1, Appendix A). Continuous measurements of velocity were included
266 due to the potential for impeded drainage under very wet conditions or caused by the accumulation

267 of snow and ice around the surface culvert in winter. An additional barometrically-corrected
268 pressure transducer (U20, Onset Ltd.) (Table A1) was also used for periods when the flow sensors
269 did not function using a rating curve developed from the depth-velocity sensors; however, it should
270 be noted that these were for brief periods and the depth-velocity sensor functioned for the majority
271 of the study. The water table elevation was measured using a barometric pressure-corrected
272 pressure transducer (U20, Onset Ltd.).

273 Air temperature, wind speed, air relative humidity, incoming solar irradiance and rainfall
274 were also measured at the site at 15-minute intervals and ~~used to fore~~were implemented in the
275 model. Variable names and their symbols in CRHM are listed in Appendix B. The air temperature,
276 wind speed and incoming solar radiance measurements were collected 1 m above ground using a
277 Temperature Smart Sensor S-THB-M002, Wind Smart Sensor Set S-WSET-M002 and a Solar
278 Radiation Sensor (Table A1). Rainfall and relative humidity were measured via a tipping bucket
279 rain gauge (Table A1) and an RH Smart Sensor (Table A1). These observations were continuously
280 recorded throughout the study period, except for brief periods of instrument failure and
281 maintenance, when data from nearby stations (Table T1, Supplementary Material) was substituted
282 using the double mass analysis method (Searcy and Hardison, 1960).

283 Although rainfall was recorded continuously at the field site, snowfall data was not.
284 Snowfall data was obtained from nearby stations (Wroxeter-Davis and Wroxeter, Environment
285 Canada, [20212020](#)), located 31.7 km from the field site. Periodic snow surveys done at the site
286 throughout the study period found that data from the nearby stations was a close approximation of
287 snow at the field site (Plach et al., 2019). Hourly snowfall observations from Wroxeter-Geonor
288 were used for the period between 2015 and 2018, whereas daily data from the Wroxeter-Geonor

289 were used for the 2011 to 2014 period, reconstructed to hourly snowfall time series based on the
290 method presented by Waichler and Wigmosta (2003).

291

292 2.4 *Development of the new tile module*

293 A Tile Drainage Module (TDM) was developed within CRHM (Figures 2, 3) with the goal of
294 adding the ability to simulate tile flow and the resulting saturated storage (~~water table~~) at an hourly
295 time step. CRHM was forced with hourly precipitation, air temperature, solar radiation, wind speed
296 and relative humidity to calculate hydrological states and fluxes in HRUs and the basin. The model
297 requires parameterizations that specify the hydraulic and hydrological properties of the soil,
298 including its thickness, saturated hydraulic conductivity (K), and surface cover. CRHM calculates
299 water storage and fluxes between HRUs, as well as vertical fluxes amongst different hydrological
300 compartments (within each HRU) that include snow, depression storage, different soil layers,
301 and groundwater.

302 Using the simulation of soil moisture (including both saturated and unsaturated soil
303 moisture) performed by the original CRHM “*Soil*” module, TDM calculates the dynamic tile flow
304 rate that, in turn, feeds back to soil moisture at each time step. The presence of a capillary fringe
305 (sometimes referred to as the tension-saturated zone within the soil profile) and its effects are
306 considered by limiting the amount of drainable soil water. TDM uses site-specific information
307 regarding the tile network, such as tile depth, diameter and spacing. Information regarding site-
308 specific details regarding tile depth, diameter and spacing may be obtained directly from
309 landowners or can be estimated based on standard design and installation guidelines for the region.
310 This information was used to set up the model together with parameterization to translate the
311 hydrological effects of the soil capillary fringe (CF), if present, through two variables, CF

312 thickness and CF drainable water (discussed in Section 2.5, Figures 2, 3). These two variables are
313 used to limit the fraction of the soil moisture that can freely drain to the tiles.

314

315 2.4.1 Soil moisture and ~~saturated storage~~~~water table elevation~~

316 The TDM uses the water quality soil module or soil module (WQ_soil or $Soil$), which divides the
317 soil column into ~~three~~~~two~~ layers: a recharge layer where evapotranspiration and root uptake
318 generally take place, ~~and~~ a deeper layer that connects to the groundwater system and a deeper
319 groundwater layer that is always saturated. ~~Since~~ CRHM's state variable for soil moisture in the
320 upper two layers is soil water storage volume (Fig. 2), the model results were converted into water
321 table elevation above the semi-permeable layer (Table B1, Appendix B; ~~see~~ Fig. 2b) for
322 comparison with water table observations,) by dividing volumetric soil moisture content (Table
323 B1) by soil porosity (Table B1) for the cases with no capillary fringe above the water table.
324 Additional steps were taken for periods when a capillary fringe developed (discussed below).

325

326 2.4.2 Capillary fringe and drainable water

327 Soil moisture in the capillary fringe is equal to the average volumetric water content at capillary
328 fringe (θ_c) which is usually greater than the field capacity (θ_{fc}) (Bleam, 2017, Sect. 2.4).
329 Therefore, while the positioning of the capillary fringe responds dynamically to the matric
330 potential, the saturation profile within the capillary fringe remains constant, as well as its thickness
331 because it only depends on the pressure head (capillary forces) that are related to the grain size
332 distribution and field capacity (h_{fc}) as introduced by ~~Twarakawi~~~~Twarakavi~~ et al. (2009).
333 Therefore, the drainable water in the capillary fringe becomes the difference between saturation
334 (θ_s), computed dynamically in CRHM, and θ_c , which corresponds to the water held by capillary

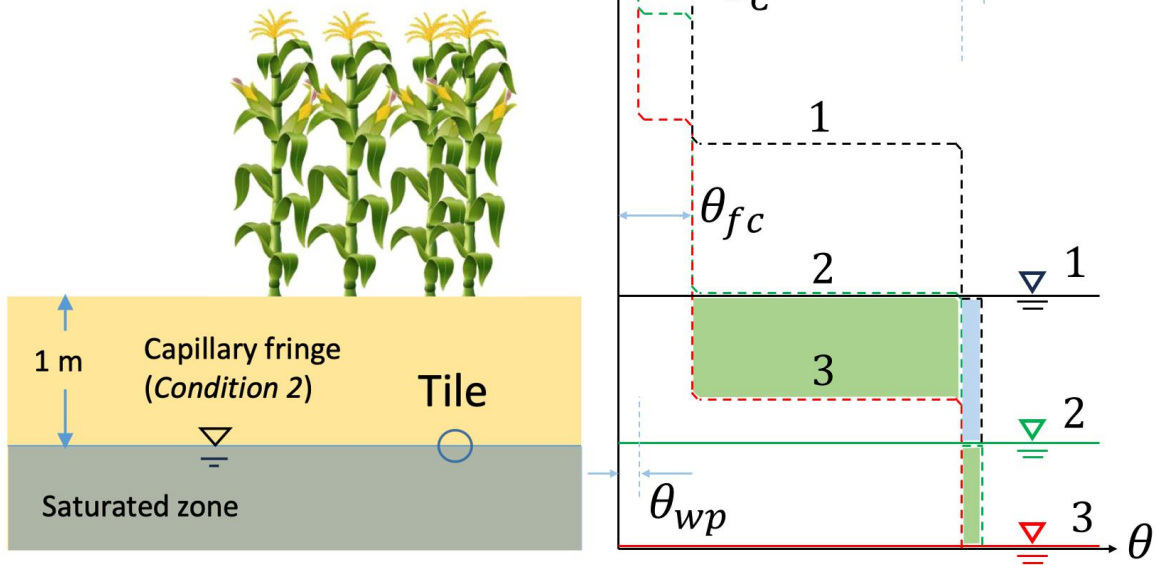
335 forces at the capillary fringe moisture content (Fig. 2). Accordingly, Fig. 2 shows the schematic
336 soil characteristic curve for the three water level conditions contemplated in the model.

- 337 1. *Condition 1* is when the water table is at the surface and the soil is completely saturated
338 (matric potential = 0);
- 339 2. *Condition 2* is when the water table drops but the upper boundary of the capillary fringe
340 is at the soil surface; and
- 341 3. *Condition 3* is when the water table drops further, and the upper boundary of the capillary
342 fringe drops beneath the surface.

343 In essence, the soil is completely saturated (θ_s) in *Condition 1*. Between *Conditions 1* and 2, the
344 capillary fringe occupies the entire soil column above the water level; thus, it can only release the
345 volume of water corresponding to $\theta_s - \theta_c$ or φ_c (dimensionless). Between *Conditions 2* and 3, two
346 layers with distinct hydraulic characteristics develop: (1) the top one at θ_{fc} that releases water up
347 to $\theta_c - \theta_{fc}$, and (2) the lower one that corresponds to the capillary fringe and can release up to the
348 volume of water corresponding to $\theta_s - \theta_c$ or φ_c .

Drained water when the water table position is changed:

- from *Condition 1* to *Condition 2*
- from *Condition 2* to *Condition 3*



349

350 Figure 2. Schematic representation of the capillary fringe above the water table assuming a 1-m thickness (for demonstration
 351 purposes). The soil characteristic curves are shown for the three water level conditions considered: water level at the (1) surface,
 352 (2) intermediate depth, and (3) deeper depth. Two transitional drops can be seen in the characteristic curves, one from saturation
 353 (θ_s) to capillary fringe water content (θ_c) (between *Conditions 1* and 2) and one from θ_c to field capacity (θ_{fc}) (between *Conditions*
 354 *2* and 3). The coloured areas (green and blue) of the right panel correspond to the amount of water that can be released between
 355 *Conditions 1* and 2 (blue) and between *Conditions 2* and 3 (green).

356

357

358 2.4.3 Tile flow calculation

359 A modified version of the Hooghoudt equation was used to calculate tile flow in the TDM
 360 (Smedema et al., 2004). This, which presumes no surface ponding, an assumption that generally
 361 holds at the study site (Eq. 1), where water ponds only during very wet periods and on a small
 362 portion of the study site (see Fig. 1b). Hooghoudt's equation (Hooghoudt, 1940) is a steady state,

363 physically based equation for saturated flow toward the tile drain. Flow estimates are provided
 364 based on the hydraulic conductivity of the soil and water table elevation above the tile pipe. It
 365 allows different saturated hydraulic conductivities for the layers above (AL) and below (BL) the
 366 tile (Fig. S1). At the study site, soil surveys have reported almost the same soil type (Loam) down
 367 to the depth of 90 cm (e.g., Van Esbroeck et al., 2016; Plach et al., 2018b), which was
 368 parameterized in the model set up as,

369

$$370 \quad q = \frac{8 \times K_2 \times d \times h}{L^2} + \frac{4 \times K_1 \times h^2}{L^2}, \quad (1)$$

371

372 where K_1 and K_2 are respectively the saturated hydraulic conductivity in the upper and lower layers
 373 in mm h^{-1} ; L is the tile spacing in mm; h is the water table elevation above the tile in mm, d is the
 374 lower layer thickness in mm (Fig. S1), and q is the predicted tile flow in mm h^{-1} . The only variable
 375 that is dynamically updated by CRHM is h . Equation (1) ~~is~~ was used to estimate ~~the~~ tile flow rates
 376 in TDM, using saturated storage to estimate h .

377

378 2.4.4 Calculation of the effect of tile flow on soil moisture and water levels

379 The simulated tile flows (see Sect. 2.3.3) ~~we~~ are subtracted from the soil moisture. To calculate
 380 saturated storage (water table or groundwater elevation head level) from soil moisture calculated
 381 by the model, a threshold soil moisture content (sm_t) is defined, which consists of drainable water
 382 in the soil (φ_c) when the upper boundary of the capillary fringe is at the surface (*Condition 2*, Fig.
 383 2) and was calculated as:

384

$$385 \quad sm_t = sm_{max} - (C_t \times \varphi_c), \quad (2)$$

386

387 where sm_{max} is the maximum soil moisture and C_t is the capillary fringe thickness in mm.

388 However, since the hydrological conditions of the soil are markedly different between the two

389 transitional situations described in Sect. 2.3.2 and Fig. 2 (*Condition 1* to 2 and *Condition 2* to 3),

390 a step function was deployed for determination of saturated storage ~~the water table elevation~~:

391

392
$$SSWT = \begin{cases} \frac{sm_t - (C_t \times ((\varphi_s - \varphi_c) + \theta_{fc}))}{\varphi_s + \theta_{fc}} + \frac{sm - sm_t}{\varphi_c} & , \text{if between Conditions 1 and 2} \\ \frac{sm_{max}}{\varphi_s + \theta_{fc}} - \left(\left(\frac{sm_t - sm}{\varphi_s} \right) + C_t \right) & , \text{if between Conditions 2 and 3} \end{cases} \quad (3)$$

393

394 where ~~WT is water table elevation (or soil SS is~~ saturated storage, ~~SSS)~~ in mm from the bottom

395 of the soil, and sm is soil moisture (both saturated and unsaturated storage) in the given time step

396 in mm. Water table observations were used to estimate SS from the field. Equation (3) is

397 determined based on soil moisture curves in Fig. 2 and water level *Conditions 1-3* discussed in

398 Sect. 2.3.2. In Fig. 2, the first and second parts of Eq. (3), which refer to *Conditions 1* to 2 and 2

399 to 3, respectively, correspond to the volumes of soil water highlighted in “blue” and “green.”

400

401 2.4.5 Lower semi-permeable soil layer and periodicity in annual groundwater levels

402 This model application focused on the study site field without including other adjacent areas. This

403 was possible because years of field monitoring at this site have demonstrated that there is no

404 observable surface flow into the site from adjacent farmsfields. The tile network is restricted to the

405 field and is not connected to tile drains or surface inlets in adjacent fields. However, field soil

406 water table observations show evidence of annual groundwater level periodicity/fluctuation (Rust

407 et al., 2019) that are sinusoidal in nature and cannot be neglected. Some studies predict the annual
 408 groundwater oscillations or the annual responses of groundwater to precipitation by using sine and
 409 cosine functions (De Ridder et al., 1974; Malzone et al., 2016; Qi et al., 2018). De Ridder et al.
 410 (1974) studied the design of the drainage systems and described the seasonal groundwater
 411 fluctuations observed in wells using sinusoidal curves. Malzone et al. (2016) used a sine function
 412 to predict annual groundwater fluctuations in the hyporheic zone. Qi et al. (2018) and Rust et al
 413 (2019) used a cross-wavelet transform, consisting of the superposition of sine and cosine curves,
 414 to predict shallow groundwater response to precipitation at the basin scale. This approach, using
 415 the sine function, was used in this application to simulate annual fluctuations in saturated
 416 storage groundwater water table, in Eq. (4), over a period of 1 year, with minimums around the
 417 middle of the growing season (mid-July), and maximums in the cold season (early February). This
 418 translates into the ~~lower~~ higher ~~greater~~ matrix potential, with soil moisture depletion, during the
 419 growing season, ~~coinciding with soil moisture depletion~~, and lower matrix potential, with soil
 420 moisture increases, ~~then~~ during the non-growing season, ~~an elevated matrix potential coinciding~~
 421 ~~with an increase in the soil moisture~~, consistent with field observations. Thus, a sine function
 422 representing the annual fluctuations in percolation rate from soil to groundwater ($G_{y,i}$) layers in
 423 CRHM, through the lower soil semi-permeable layer (in mm hr^{-1}) is defined as:

424

$$425 \quad G_{y,i} = \left[A \times \sin \left(\frac{(T_s - D_d \times 24) \times 360}{24 \times 365.25} \right) - B \right] \times f_{y,i} \quad (4)$$

426

427 where T_s is the time step number, D_d is a time delay in days, A is the amplitude of the water
 428 table saturated storage (WTSS) fluctuation, and B is an intercept factor. $f_{y,i}$ is a seasonal factor.

429 The sine function coefficient (D_d , A , and B) and seasonal factor were adjusted for the whole period

430 and for each year through model verification and shown in Table 1. Appendix C provides more
431 details on the implementation of Eq. (4). Although this is a simplification of the entire groundwater
432 system dynamics, it was needed here to provide a more controlled basis for testing the new module
433 at the field scale before expanding it to larger areas in future work.

434

435 2.5 Model application and multi-variable, multi-metric validation

436 The study site is a relatively small field, and 2 HRUs were sufficient to capture its hydrological
437 dynamics in CRHM. The HRUs represent (1) the area immediately upstream of the outlet where
438 surface ponding occurs (depression storage); and (2) the remaining field (Fig. 3). The maximum
439 ponding capacity of HRU 1 was estimated using the spatially distributed hydrodynamic model
440 FLUXOS-OVERFLOW (Costa et al., 2016, 2020b). The CRHM model with its new TDM module
441 were set up using the information described in Table 1. Soil textures at the LON site measured
442 in a 25 m grid across three soil depths (0-25 cm, 25-50 cm, and 50-100 cm) averaged 29% sand,
443 48% silt, and 23% clay (Ontario Ministry of Agriculture, Food and Rural Affairs Soil Team,
444 unpublished data). This soil grain size distribution corresponds with a soil-soil-saturated hydraulic
445 conductivity of $\sim 0.56 \text{ cm h}^{-1}$ ($\sim 10^{-2.5}$) (Garcia-Gutierrez et al., 2018), which was implemented
446 in CRHM (0.5 cm h^{-1}), corresponding to a field capacity of 0.04 (volumetric water content) and
447 h_{fc} of $\sim 0.8 \text{ m}$ (Twarskawi-Twarskavi et al., 2009, based on a drainage flux of 0.1 cm d^{-1}).

448

449 A robust multi-variable, multi-metric model evaluation strategy was deployed to verify the
450 capacity of the model to predict tile flow and its impact on the local hydrology. The outflows
451 examined were tile flow, surface flow, and saturated storage water table depth. The multi-metric
452 approach contemplated five different methods, namely the Nash-Sutcliffe efficiency (*NSE*), Root-

453 Mean-Square Error (RMSE), Model Bias (Bias), Percentage Bias (Pbias), and RMSE-observation
454 standard deviation ratio (RSR). [These methods were used to assess model accuracy.](#) See Appendix
455 C for more details about the methodology used. It is generally assumed that $NSE > 0.50$, $RSR \leq$
456 0.70 , and $PBias$ in the range of $\pm 25\%$ are satisfactory for hydrological applications (Moriassi et
457 al., 2007). Five different metrics were used to evaluate model accuracy in order to describe
458 different aspects of the discrepancies between simulated and observed values. For example, Bias
459 reveals the positive or negative general deviations of simulated values from the observed values,
460 while RMSE shows the average absolute differences between them (Moriassi et al., 2007). Hourly
461 values were used in these calculations, which departs from the daily and monthly analyses typically
462 reported for these types of models. Although the hourly timestep is challenging for this sort of
463 simulation, it is an important advance forward toward more detailed, accurate, and advanced
464 models for ~~tile-tile~~-drained agricultural fields. For example, Costa et al., (2021) noted that the
465 successful extension of hydrological models to water quality studies relies on their ability to
466 operate at small time scales in order to capture intense, short-duration storms that may have a
467 disproportional impact on the runoff transport of some chemical species such as phosphorus – in
468 essence, to capture hot spots and hot moments for flux generation.

469

470 Table 1. Key model parameters in CRHM for representation of the LON site.
471

Model Parameter	Value	Unit	Source	Adjusted/Calibrated	Comment
Soil depth or Soil thickness, T_{SL}	2	m		No	Assumed
Semipermeable layer depth	3	m		No	Assumed
Tile depth	0.9	m		No	Farmer/Blueprints of the field
Corn root depth	0.5	m		No	Online sources

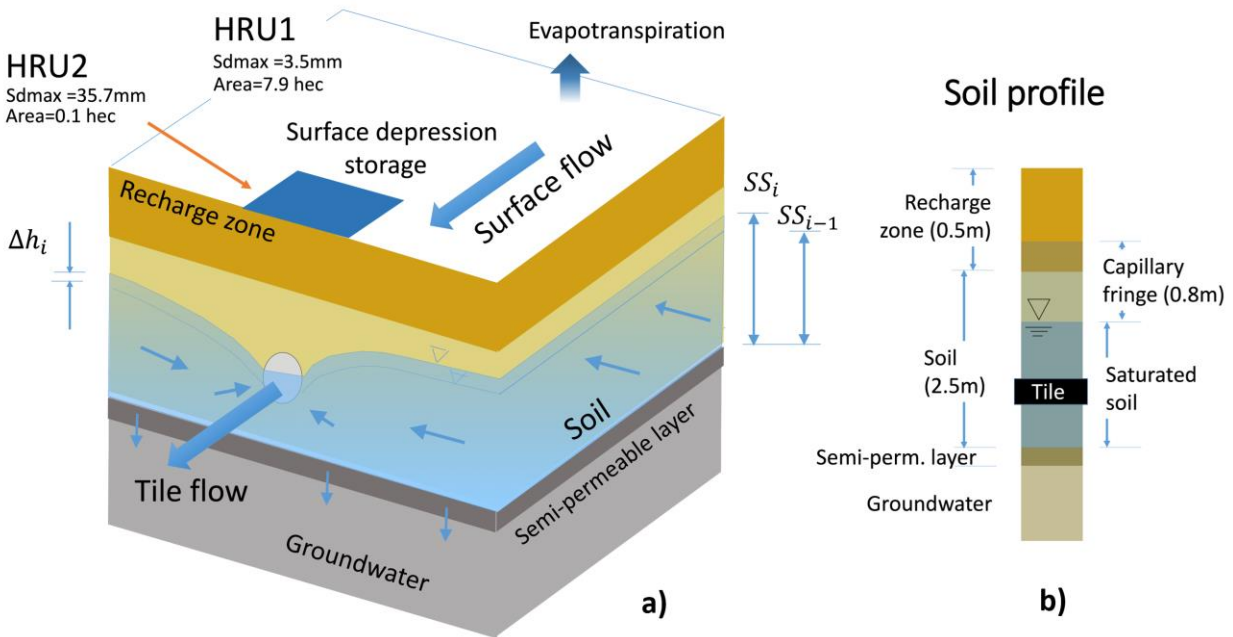
Soil recharge zone thickness	0.5	m	No	Based on the root depth
Tile spacing	14	m	No	Farmer/Blueprints of the field
Soil porosity (soil drainable water) φ_s	0.045		Yes	Adjusted
Saturated Hydraulic conductivity, K_s in lower soil layer	5	mm h ⁻¹	Yes	Adjusted
K_s in upper soil layer	5	mm h ⁻¹	Yes	Adjusted
Capillary fringe thickness, T_{CF}	0.8	m	Yes	Adjusted
Capillary fringe drainable water, φ_C	0.03		Yes	Adjusted
Surface depression close to farm surface flow outlet (HRU2)	35	mm	Yes	Calculated
Surface depression in rest of the field (HRU1)	0	mm	No	Calculated
Surface area of HRU1	79000	m ²	No	Field observations and DEM
Surface area of HRU2	1000	m ²	No	Field observation and DEM
Soil module name in CRHM	WQ_soil		No	
Infiltration module name in CRHM	GreenAmpt		No	
Soil type in GreenAmpt module	5		Yes	Adjusted
Saturated K in GreenAmpt module	6	mm h ⁻¹	Yes	Adjusted
Soil wilting point	0.025		Yes	Adjusted
A_s in sine function	0.025	mm h ⁻¹	Yes	Adjusted
B_s in sine function	-0.005	mm h ⁻¹	Yes	Adjusted
D_d in sine function	15	d	Yes	Adjusted
$f_{2012,2}$ (Seasonal factor, sine function)	2.0		Yes	Adjusted
$f_{2015,2}$ (Seasonal factor, sine function)	1.8		Yes	Adjusted
$f_{2016,2}$ (Seasonal factor, sine function)	2		Yes	Adjusted

$f_{2017,2}$ (Seasonal factor, sine function)	1.4	Yes	Adjusted
$f_{y,i}$	1	No	By default for $y =$ 2012 to 2017 and $i = 1, 2$

472

473

474



475

476 Figure 3. a) Schematic conceptual view of the CRHM model configuration, including soil layers, [water table saturated storage](#)
477 ([WTSS](#)), groundwater, and tile flow.; and b) soil profile, including the capillary fringe and its location relative to the soil and tile.

478

479 3. Results

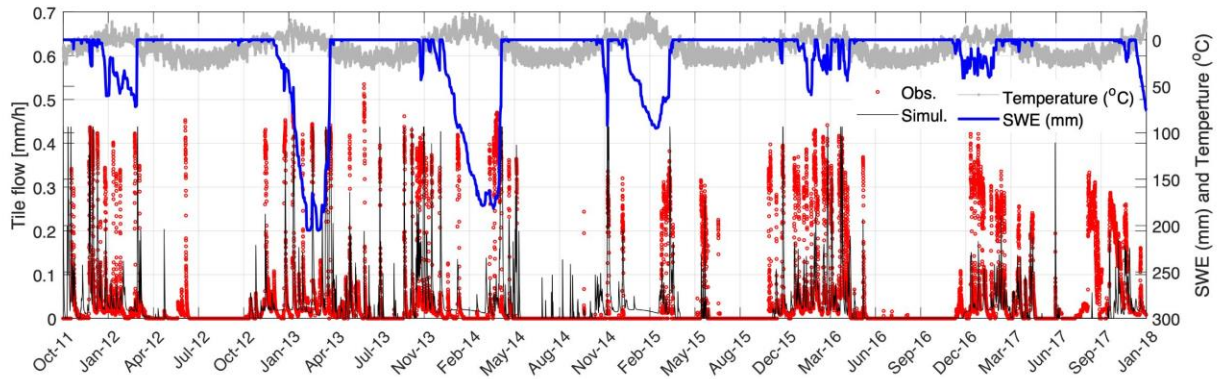
480 [A multi-variable, multi-metric model evaluation approach was deployed to verify the capacity of](#)
481 [the model to predict not only tile flow but also the effects it has on the local hydrology, from](#)
482 [surface to sub-surface processes. The outflows examined were tile flow \(Section 3.1\), **saturated**](#)
483 [storage **water table depth** \(Section 3.2\), and surface flow \(Section 3.3\). The multi-metric approach](#)

484 contemplated five different methods, namely the Nash-Sutcliffe efficiency (NSE), Root-Mean-
485 Square Error (RMSE), Model Bias (Bias), Percentage Bias (Pbias), and RMSE-observation
486 standard deviation ratio (RSR).

487 3.1 *Tile flow*

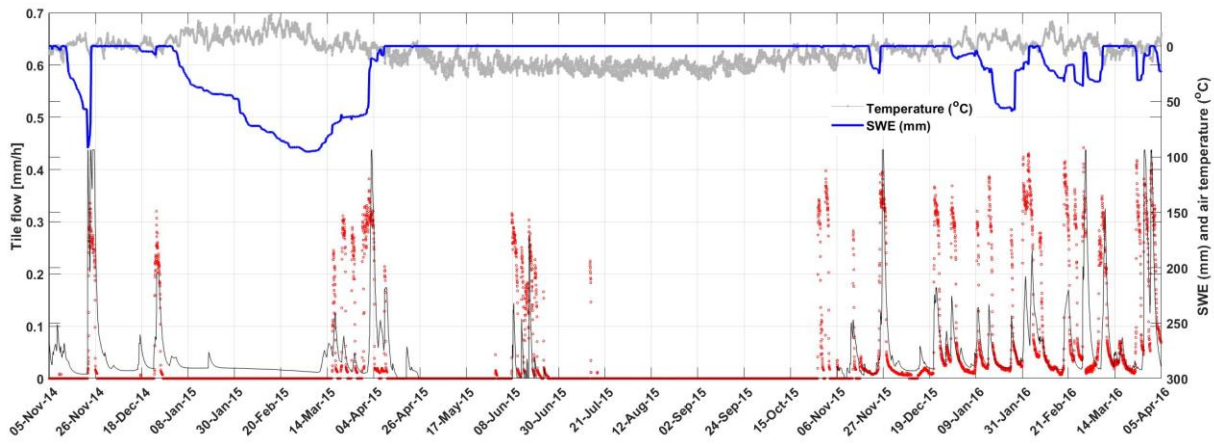
488 The model was able to capture most tile flow events, both in terms of the timing and magnitude of
489 peak flows and the most important seasonal patterns (Fig. 4). For example, the ~~almost complete~~
490 ~~absence of tile~~near absence of flow during the growing season (May to September) was captured.
491 The simulated flow peaks generally had a good agreement with observations, as well as the low
492 flow or base flows during cold periods (December-March). The ascending and descending limbs
493 of the response signal were also adequately predicted.

494
495 Results show that tile flows generally occurred during snowmelt events, as indicated by the
496 synchrony between snow water equivalent (SWE) depletion and tile flow. The maximum
497 snowpacks (or snow water equivalent, SWE) were markedly smaller during the winters of 2016
498 and 2017 when compared with those of 2013 to 2015. However, this did not necessarily translate
499 into lower tile flows as precipitation also occurred as rain during these seasons. Although ~~the~~
500 ~~magnitude of peak~~ tile drainage flow peaks was not always predicted accurately, the model was
501 able to capture the annual trends of both an absence of tile flow during the summer months
502 (growing season) and the ascending and descending limbs of the tile hydrograph during events
503 (Figure 4).



504

505 a)



506

507 b)

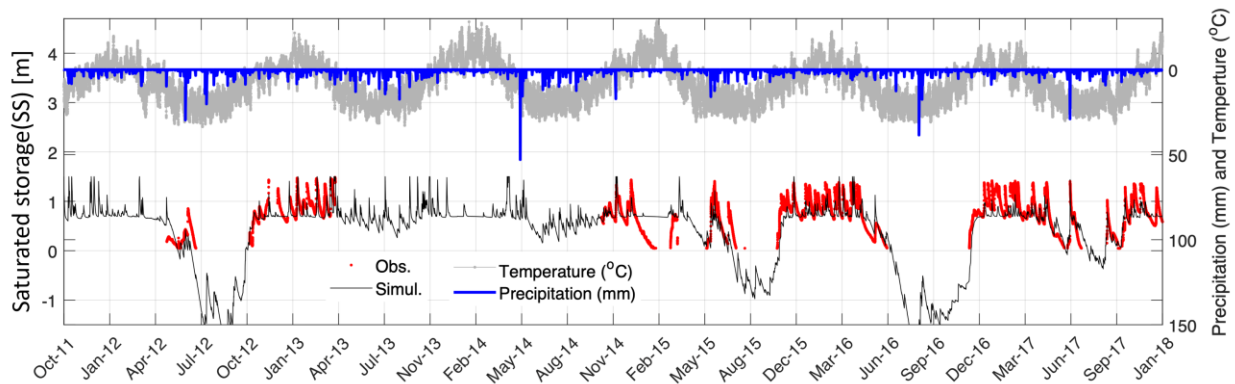
508 Figure 4. Comparison between observed and simulated tile flows, simulated SWE (snow water equivalent), and observed air
 509 temperature in the LON site, between October 2011 to January 2018 (a) and between November 2014 to April 2016 (b).

510

511 3.2 ~~Water table or s~~Soil saturated storage

512 Simulated and observed soil saturated storage ~~and the observed water table~~ are compared in Fig.
 513 5, alongside air temperature and precipitation observations. Despite the gaps in the observational
 514 record during two periodic equipment failures, the model agrees well with observations. Above
 515 tile drains, ~~water table~~ fluctuations in saturated storage were controlled by infiltration/recharge,
 516 tile flow, groundwater flow, and matric potential that affect the drainable water from the capillary

517 fringe. This caused flashier storage responses above the tile that were captured well by the model.
 518 In contrast, tiles did not withdraw water from the soil layer below the tile pipe and thus did not
 519 control ~~water table~~ fluctuations in saturated storage when levels were below the drain pipe, and
 520 tile drains did not flow during such periods. During the growing season, both the observed and
 521 simulated ~~water table (or saturated storage)~~ dropped abruptly because of the seasonal lowering of
 522 the regional groundwater water table. In the growing seasons of 2012, 2015 and 2016, which were
 523 dry years, large declines in ~~the water table and~~ saturated storage were observed, whereas in wetter
 524 years such as 2013 and 2014, seasonal saturated storage water level declines were smaller. The
 525 seasonal declines in saturated storage water level during the growing season led to a cessation in
 526 tile flow in most years (Fig. 4, 5), even following rainfall events. For example, there was a large
 527 precipitation event (~35 mm) in the growing season of 2016 that did not produce tile flow (apparent
 528 in both model and observations).

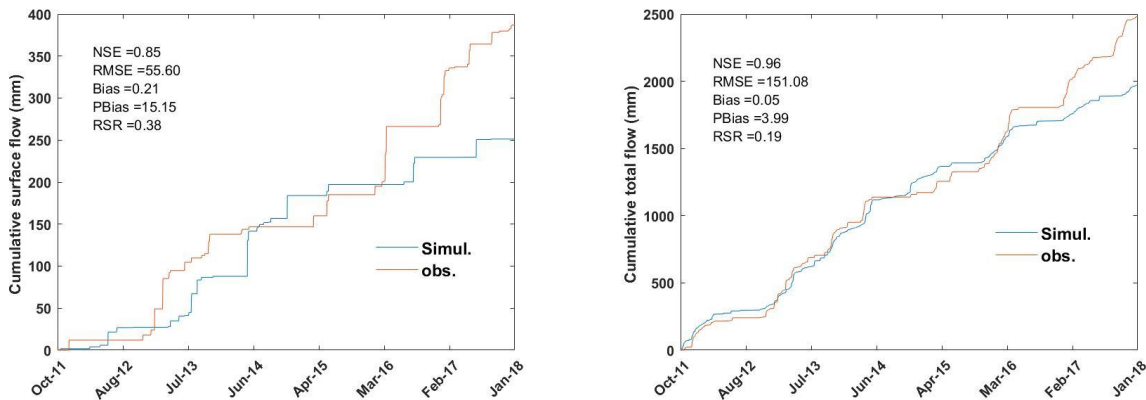


529
 530 Figure 5. Time series of the simulated and observed saturated storage ~~and (or observed water table)~~ in the soil or groundwater
 531 layers of the model along with the observed temperature and precipitation. ~~Given that tiles do not flow when the WT is below them,~~
 532 ~~the WT = 0 when the water table elevation is at the depth of the tile drainpipe. In the figure, the water table is measured as the~~
 533 ~~elevation above (+) or below (-) the tile pipe.~~

534

535 3.3 Surface flow and total flow

536 The model was not always able to capture the observed surface flow as satisfactorily as it captured
537 tile drainage (Fig. 6a). Some possible reasons are uncertainties in the measurements of surface
538 flow due to ponding in surface depressions on the field, which impeded the drainage of some of
539 the surface runoff prior to ~~when it exit~~inged the field through the culvert (see Fig. 1), or uncertainty
540 in field estimates of SWE. However, the model performance improvesd considerably when both
541 runoff and tile flow were combined (referred to as total flow, Fig. 6b). Indeed, most of the flow
542 from the field was through tile drains (80% in 5-year average) rather than surface runoff (20% in
543 5-year average, Plach et al., 2019). The underestimation of both cumulative total and surface flows
544 during 2017 and 2018 is possibly due to the removal of the blockage in the tile pipe in early 2017,
545 which may have affected both surface and tile flow. The differences in timing of the simulated and
546 observed surface flow for many of the main events (Figure 6) shows that there remain systematic
547 issues in simulation of surface flow by CRHM which should be addressed in future research.



(a)

(b)

548 Figure 6. Observed and simulated cumulative surface flow (a) and total flow (b).

549

550 3.4 Overall model performance

551 The model performance was calculated based on hourly data for various model outputs (Table 2).
552 To compare the performance of the model in different seasons we calculated the coefficient for
553 wholeentire year as well as separately for the growing and non-growing seasons~~separately~~. The
554 results confirm that ~~for the whole year~~ the model is robust over an annual cycle in the sense that it
555 can capture the main patterns of tile flow, surface flow, and ~~saturated storage~~~~water table elevation~~.
556 The Pbias values are below 25% for most of the fluxes and cumulative fluxes. The RSR values are
557 also generally below 1.0. The NSE values are positive and above 0.3 for most fluxes, except for
558 surface flow, where the model exhibited some difficulties. The weaker performance of the model
559 in the simulation of surface flow, which is illustrated by the NSE coefficient, can be partly related
560 to difficulties in measurement of surface flow during flooding, ponding, and freeze ~~and~~ thaw on
561 the surface. The performance coefficients were calculated for the growing season, May-
562 September (Table 2b) and non-growing season, October-April (Table 2c). The results shows that
563 surface flow biases are significantly larger and negative in May-September and are smaller and
564 positive during October-April. For tile flow the ~~Biases~~~~biases~~ are a bitslightly higher in May-
565 September ~~while~~~~whereas~~ for ~~saturated storage~~~~oil water table~~ and total flow the biases are a
566 bitslightly lower in May-September. The NSEs are more acceptable in October to April for surface
567 flow, tile flow and total flow, but the NSE for ~~WT-SS~~ is more acceptable in May-September. The
568 overall performance of the model for both tile and surface flow is more reliable in the non-growing
569 season, when the regional water table was above the tile and saturated storage ~~the water level~~
570 fluctuations ~~was~~~~were~~ mainly controlled by tile flow rather than regional groundwater oscillations.

571

572 Table 2. Performance coefficients for surface flow, tile flow and ~~water tablesaturated storage~~ (WFSS/SSS), as well as total (tile +
573 surface) flow, for the simulation period of October 2011 to January 2018. The coefficients were calculated for both hourly and

574 daily flow rates, for the whole year (a) for May to September (b) and for October to April (c). (Green and red color show the
 575 seasonal coefficients improved and worsened, respectively, -compared to their seasonal values).

576 a) Coefficients for whole year

Performance coefficients	Surface flow	Tile flow	WT (m)SS	Total flow	
NSE*	-2.29	0.31	0.49	-1.38	Coefficients calculated for hourly flow rates (mm h ⁻¹)
RMSE [^]	0.27	0.08	0.26	0.30	
Bias [#]	0.54	0.24	0.14	0.28	
Pbias ^{\$}	21.77	17.91	10.46	18.63	
RSR ^{&}	1.82	0.83	0.71	1.54	
NSE	-0.73	0.29	0.50	0.01	Coefficients calculated for daily flow rates (mm d ⁻¹)
RMSE	2.04	1.72	0.24	2.92	
Bias	0.35	0.20	0.09	0.22	
Pbias	35.11	19.63	9.33	21.73	
RSR	1.31	0.84	0.70	0.99	

577

578

579 b) coefficients for May to September

Performance coefficients	Surface flow	Tile flow	WT (m)SS	Total flow	
NSE*	-18.98	0.19	0.40	-11.76	Coefficients calculated for hourly flow rates (mm h ⁻¹)
RMSE [^]	0.26	0.03	0.12	0.26	
Bias [#]	-1.43	0.49	0.03	0.11	
Pbias ^{\$}	-142.79	48.88	3.44	10.96	
RSR ^{&}	2.85	0.57	0.39	2.27	
NSE	-3.89	0.21	0.41	-1.08	Coefficients calculated for daily flow rates (mm d ⁻¹)
RMSE	1.39	0.73	0.11	1.66	
Bias	-1.43	0.49	0.02	0.11	
Pbias	-142.79	48.88	2.07	10.96	
RSR	1.41	0.56	0.39	0.92	

580

581 c) coefficients for October to April

Performance coefficients	Surface flow	Tile flow	WT (m)SS	Total flow
--------------------------	--------------	-----------	-------------	------------

NSE*	-0.37	0.24	0.20	-0.04	Coefficients calculated for hourly flow rates (mm h ⁻¹)
RMSE [^]	0.11	0.07	0.21	0.14	
Bias [#]	0.87	0.14	0.11	0.24	
Pbias [§]	86.59	13.56	11.00	24.11	
RSR ^{&}	0.90	0.67	0.77	0.79	
NSE	-0.11	0.26	0.24	0.18	Coefficients calculated for daily flow rates (mm d ⁻¹)
RMSE	1.50	1.56	0.21	2.40	
Bias	0.87	0.14	0.11	0.24	
Pbias	86.59	13.56	10.58	24.11	
RSR	0.81	0.67	0.75	0.70	

582

583

584

585

586 *Nash-Sutcliffe efficiency, ^Root-Mean-Square Error, #Model Bias, §Percentage Bias, &RMSE-observation standard deviation ratio

587

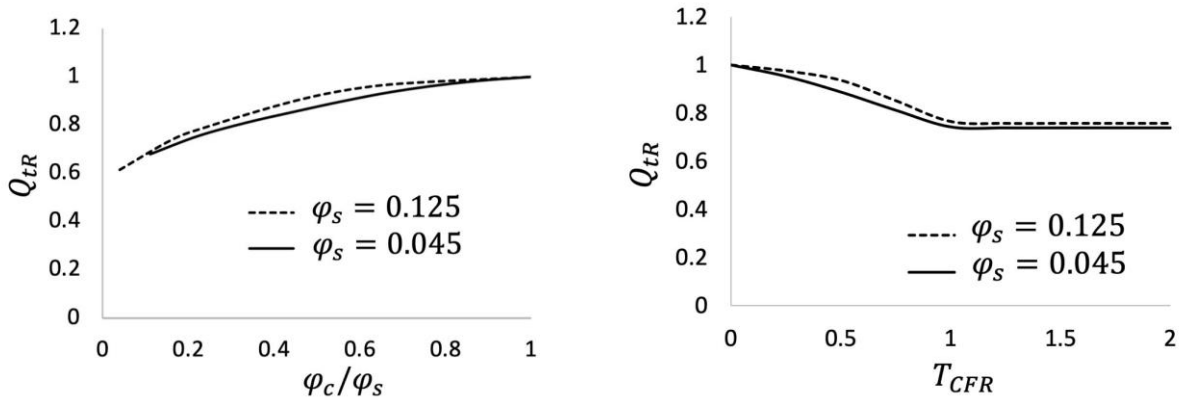
588 3.5 Presence of capillary fringe: effects and hypotheses

589 Results show that the thickness and vertical positioning of the capillary fringe ~~have had~~ a strong
590 impact on the amount of drainable soil water that ~~can flow~~ed into the tiles. To investigate this
591 effect further, the response of tile flow and soil moisture to changes in the capillary fringe was
592 examined. It should be noted that although this thickness may change slightly depending on the
593 soil type and water retention curves (Skaggs et al., 1978), the model assumed a constant value
594 given the field-scale nature of the simulations and myriad of processes contemplated. However,
595 despite the simplification, the vertical positioning of the capillary fringe was still calculated and
596 enabled a dynamic (time-dependent) calculation of the drainable soil water that was available for
597 tile drainage over time.

598

599 *Effect of capillary fringe on tile flow*

600 Figure 7a relates the simulated normalized total cumulative tile flow (Q_{tR} , total tile flow divided
601 by the total tile flow when there is no influence of capillary fringe) to capillary fringe drainable
602 water ($\varphi_{CR} = \varphi_c / \varphi_s$) for two different φ_s values (0.045 and 0.125). The values were normalized
603 (0 – 1 scale) for comparison purposes. As expected, the model indicates that tile flow increases
604 with drainable water, but the relationship is non-linear, likely because as tile carrying capacity is
605 exceeded more frequently, there is more opportunity for groundwater seepage and
606 evapotranspiration. The direct effect of φ_s (comparing the solid and dashed lines) on tile flow is
607 small because the amount of water that can effectively drain to the tile is controlled by the capillary
608 fringe and the associated drainable soil water. Figure 7b looks at the impact of the capillary fringe
609 thickness on tile flow. Here, the values are also normalized. Results show that Q_{tR} decreases with
610 increasing normalized thickness of the capillary fringe, T_{CFR} ($\frac{T_{CF}}{D_t}$, capillary fringe thickness
611 divided by tile depth), but only while the T_{CFR} is less than 1 that is when the capillary fringe
612 position is above the tile but has not reached the soil surface. Beyond this point, increments in the
613 capillary fringe thickness have no impact on tile flow because *Condition 1* has been reached (see
614 Fig. 2), which essentially means that the capillary fringe has reached the soil surface. The match
615 between the curves for two different φ_s values shows that the changes in φ_s does not influence the
616 effect of normalized capillary fringe thickness and drainable water on normalized tile flow. In
617 Appendix D the sensitivity of cumulative tile flow and mean saturated storage soil-water table
618 elevation to different parameters are shown along with general approaches for evaluation of the
619 model parameters for new sites, the site with no tile flow and water table observations.



a)

b)

620 Figure 7. Comparison between normalized tile flow (Q_{tR}) and (a) normalized drainable soil water (φ_c/φ_s) and (b) capillary fringe
 621 thickness (T_{CFR}) for different maximum soil saturation values (φ_s), by drawing the model prediction lines.

622

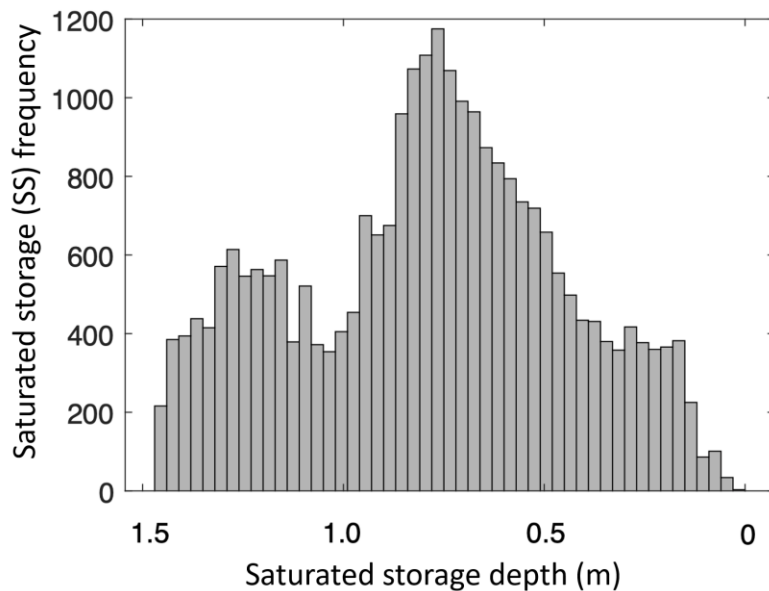
623 *Effect of capillary fringe on soil moisture*

624 Observations and ~~simulations of saturated storage model results of WT~~ reveal a bimodal frequency
 625 distribution (Fig. 8 and 9, respectively) with peaks at 0.85 m and 1.25 m depth, with the former
 626 corresponding to the ~~influenced depth~~ of the tile pipe and the second peak reflecting that from the
 627 capillary fringe ~~thickness~~. ~~In~~ I simulated soil saturated storage (~~SSS as a measure of WT~~) frequency
 628 distributions (Fig. 9), ~~show a the~~ first peak that highlights ~~again~~ the efficiency of the tile in
 629 removing soil moisture. In contrast, the second peak indicates a strong model response to
 630 differences in the capillary fringe thickness. It shows that when there is near-constant percolation
 631 from the bottom of the soil layer, the matric potential varies the greatest while it remains between
 632 the tile depth and the soil surface. While the ~~saturated storage water table~~ fluctuates faster and is
 633 more unstable within this range, it also remains there for shorter periods. This bimodal response
 634 tends to push the ~~saturated storage layer water table depth~~ below the tile. In Figure 9, ~~we can see~~
 635 ~~that~~ the first peak happens at 0.9 m depth where the tile pipe is located, and the second peak
 636 happens at the depth equal to capillary fringe thickness. In Figure 9 the second peak is more clearer

637 for the capillary fringe thickness of more than 1000 mm. The first peak in the observed ~~water table~~
638 ~~saturated storage~~ frequency plot (Figure 8) happened around 0.8 m which almost matches with the
639 tile depth. And the second peak happened at the depth of ~1.2 m which shows that the capillary
640 fringe thickness should be around 1.2 m. But, to have a more reliable estimate for the capillary
641 fringe, based on Figure 8, data is needed at depths greater than 1.5 m.

642

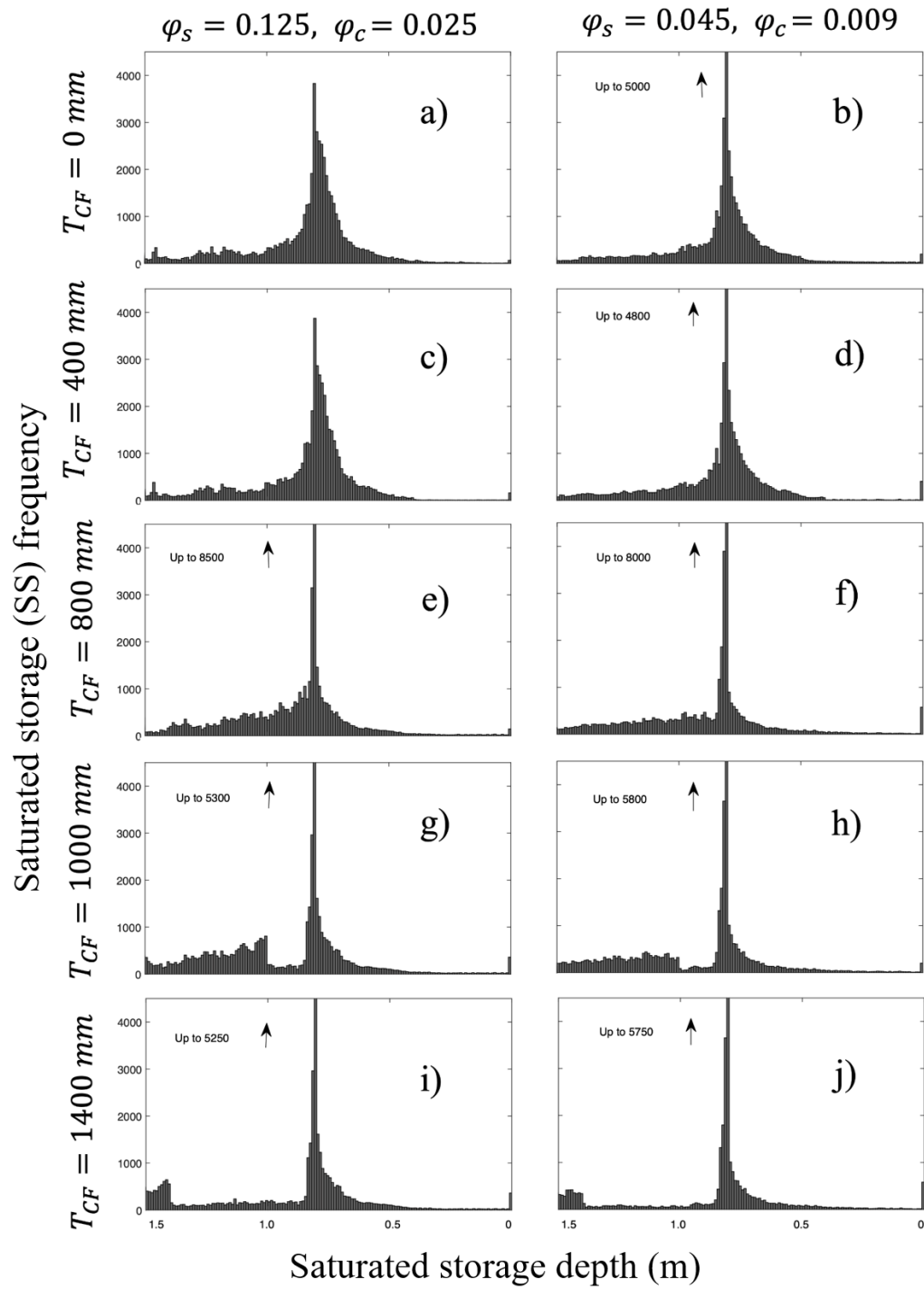
643 The bimodal behaviour of the observed ~~water table and~~ and simulated saturated storage (~~observed~~
644 ~~saturated storage is the observed water table~~) demonstrated here provides the opportunity to
645 quantify the thickness of the capillary fringe using continuously monitored ~~saturated storage water~~
646 ~~table elevations~~. The capillary fringe thickness determined using this method can then be used as
647 an input to the TDM module.



648

649 Figure 8. Histogram of the observed ~~saturated storage (or observed water table)~~ distribution for the period pf 2011 to 2018 in LON
650 (Londesborough).

651



652

653 Figure 9. Histograms of the simulated soil saturated storages versus saturated storage depth (~~SSS or WT~~) for the capillary fringe
 654 thicknesses of 0 (a,b), 400 (c,d), 800 (e,f), 1000 (g,h) and 1400 (I, j) mm and for the φ_s and φ_c of 0.125 and 0.025 (left column) as
 655 well as 0.045 and 0.009 (right column).

656

657 4. Discussion

658

659 4.1 Insights into key control mechanisms of tile flow ~~for catchment scale~~ for model simulations

660 The model suggests that tile flow may not be accurately predicted exclusively based on the soil's
661 saturated storage ~~the water table depth~~ and ~~soil~~-saturated hydraulic conductivity as suggested by
662 the steady-state flow assumptions of the Hooghoudt's equation (Hooghoudt, 1940). These results
663 indicate two additional controls: (1) the amount of drainable soil water in the soil, which has also
664 been identified in some field studies (*e.g.*, Skaggs et al., 1978; Moriasi et al., 2013) and (2)
665 fluctuations in saturated storage ~~the groundwater table (GWRD)~~ are important to account for in
666 ~~catchment scale~~ simulations. However, the relationship between drainable water and tile flow rates
667 is non-linear, as demonstrated in Fig. 7a. This is because the residence time for groundwater
668 seepage and evapotranspiration increases when the hydraulic tile carrying capacity is exceeded.
669 Comparatively, the effect of soil drainable water, φ_s (see also Fig. 7a) on tile flow is small because
670 the capillary fringe and associated drainable soil water control the amount of water that can
671 effectively flow to the tile.

672

673 The verification of the model also indicated that the slopes of the rising and falling limbs of tile
674 flow hydrographs and saturated storage ~~WT~~ were very sensitive to (1) the ratio between K_s ~~K~~ and
675 drainable soil water; and (2) the net outflow in the soil through tile flow and ~~groundwater level~~
676 fluctuations in saturated storage ~~(GWRD)~~. This is supported by previous studies showing rapid
677 responses of tile flow to precipitation events (Gentry et al., 2007; Smith et al., 2015) and others
678 that have related rapid responses in tile discharge to antecedent moisture conditions (Macrae et al.,

679 2007; Vidon and Cuadra, 2010; Lam et al., 2016a; Macrae et al., 2019), which can be affected by
680 the development of a capillary fringe and its non-drainable water.

681

682 Results show that large fluctuations in saturated storage ~~WT SS (or SSSWT)~~ and tile flow during
683 the cold season, when the water table tends to be above the tile, are primarily triggered by the
684 development of a capillary fringe that reduces the amount of drainable soil water. Model sensitivity
685 tests showed that a small amount of drainable soil water produces steeper rising and falling
686 responses (and with larger fluctuation amplitudes) in both the ~~water table (saturated storage)~~ and
687 the tile flow. Indeed, this pattern can be observed by exploring differences in tile drain responses
688 in clay loam soils with larger field capacities (and correspondingly smaller drainable water) and
689 smaller hydraulic conductivity which are more likely to experience pronounced oscillations (*e.g.*,
690 steeper rising and falling response curves) compared to tile drain responses of sandy soil, which is
691 characterized by reduced capillary forces, lower field capacities (but correspondingly larger
692 drainable water) and higher hydraulic conductivity. Notably, both model and observations of
693 saturated storage ~~WT SS (as a proxy for soil moisture)~~ reveal a bimodal (*i.e.*, two peaks) frequency
694 distribution when examined in relation to the tile depth and capillary fringe thickness (Fig. 8 and
695 9, respectively). The two peaks (*i.e.* most frequently observed saturated storage ~~WT or SSS~~
696 ~~conditions~~) correspond with the (1) depth of the tile pipe (0.75 m), which demonstrates the efficacy
697 of the tile at rapidly removing excess soil water, and the (2) the capillary fringe thickness (for the
698 depths of 1.0 and 1.4 m, Figs. G, h, I and j) beyond which the amount of drainable water above the
699 water table significantly increases.

700

701 These findings align well with studies such as Lam et al. (2016a) that recorded soil moisture near
702 saturation after tile flow had ceased, suggesting the development of a capillary fringe. Combined
703 experimental and modeling works, such as in Moriasi et al. (2013) and Logsdon et al. (2010), also
704 discuss the impact of drainable soil water (“drainable porosity” or “specific water yield”) on tile
705 flow and note that the drainable water is, in turn, dependent on the soil type, soil-water dynamic
706 and water table depth. However, these studies did not explore the dynamic nature of the capillary
707 fringe and its thickness relative to the soil column above in determining the transient amount of
708 drainage soil water that will impact the saturated storage frequency ~~WT~~ distribution and tile flow
709 differently over time (*Conditions 1 to 3*, see Fig. 2). Herein, while a capillary fringe with a fixed
710 thickness that is generally related to the soil properties was assumed, its vertical positioning was
711 simulated dynamically, which allowed determining the drainable soil water based on the evolution
712 of pressure head corresponding to field capacity. Thus, the development of the TDM has provided
713 a step forward in the modeling of tile drainage and suggests that in loam soils such as those at the
714 study site, the effects of a capillary fringe on tile flow should be included. Soil moisture (soil
715 unsaturated storage) measurements from the study site by Van Esbroeck et al., (2017) between
716 November 2011 and May 2014 from depths of 10, 30, and 50 cm (using EC-5 Soil Moisture Smart
717 Sensor) showed that almost 90% of the gravitational soil moisture drains out with 0.5 to 2.5 h.
718 ~~This~~ suggests that the saturated storage ~~water table~~ and capillary fringe can reach an equilibrium
719 condition within one hour at this field site, enabling ~~the us to use~~ of a steady state equation
720 (Hooghoudt, 1940) to predict the dynamic behaviour of the water table fluctuations.

721

722 4.2 Importance of capturing seasonal patterns in ~~saturated storage groundwater~~ to improve
723 tile flow predictions

724 The ~~saturated storage GWRD~~ changed dramatically between seasons affecting soil
725 moisture (both saturated and unsaturated storage ~~in~~ the soil) and tile flow patterns. Both
726 observations and model results show that low precipitation and higher evapotranspiration rates
727 tend to produce little tile flow during the growing season. These seasonal patterns in precipitation
728 and evapotranspiration are accompanied by a reduction in soil moisture (both unsaturated ~~storage~~
729 and saturated ~~storage~~) that leads to a substantial storage capacity in fields. Even following
730 moderate and high-intensity storms during the growing season, rapid soil moisture increases ~~are~~
731 observed (both saturated and unsaturated soil storage); however, tile flow rarely developed ~~due~~
732 to higher evapotranspiration and a seasonal decrease in the saturated storage GWRD, suggesting
733 that the soil is able to hold the water (Lam et al., 2016a; Van Esbroeck et al., 2016). In contrast,
734 tile flow ~~was~~ often observed during the cold season, with significantly smaller evapotranspiration
735 fluxes, even during smaller rainfall-runoff and snowmelt events because of reduced soil storage
736 but also a seasonal increase in regional groundwater table GWRD (Lam et al., 2016a; Macrae et
737 al., 2007, 2019; Van Esbroeck et al., 2016). This concurs with several studies throughout the Great
738 Lakes and St. Lawrence region that have reported stronger tile responses during the non-growing
739 season, with the summer months often showing little to no tile flow (Lam et al., 2016a, 2016b;
740 Jamieson et al., 2003; Macrae et al., 2007; Hirt et al., 2011; King et al., 2016; Van Esbroeck et al.,
741 2016; Plach et al., 2019).

742 These results (the controlling effect of soil drainable water and saturated storage
743 groundwater level fluctuations on tile flow) suggest that while soil moisture (both saturated and
744 unsaturated storage) is largely controlled by tile flow rather than saturated storage GWRD in the

745 cold season, this reverses in the growing season (*i.e.*, soil moisture controls tile flow), with soil
746 moisture (both saturated and unsaturated storage) being also impacted by evapotranspiration. The
747 controlling effect of groundwater fluctuations in the growing season has also been studied by
748 Hansen et al., (2019). The model indicated that the rapid drops in observed saturated storage ~~WT~~
749 during the growing season could not be explained by evapotranspiration alone ~~as well as the crop~~
750 ~~root depths~~, thus pointing to the role of saturated storage ~~GWRD.~~. Johnsen et al. (1995) and Akis
751 (2016) also showed that the effect of groundwater accretion was more effective on tile flows than
752 surface runoff. Also, Vaughan et al. (1999) found that tile drain flows in their study site in San
753 Joaquin Valley of California were better explained and related to nonlocal groundwater appearance
754 than to local variations in irrigation amount, evapotranspiration, variation in water storage or tile
755 drain blockage. Thus, it was determined ~~that~~ in that in addition to soil saturated hydraulic
756 conductivity and soil thickness, the seasonal ~~groundwater~~ fluctuations in saturated storage and
757 capillary fringe drainable water are other important controlling factors on tile flow rates.

758

759 **5. Conclusions**

760 A new tile drain module within the modular Cold Regions Hydrological Modelling (CRHM)
761 platform has been created and tested at the field scale to support the management of agricultural
762 basins with seasonal snow covers. The model was tested and validated for a small working farm
763 in southern Ontario, Canada, and presents a step forward in the dynamic simulation of tile flow
764 and its effects on the hydrological cycle in cold climates. Observations and model results showed
765 that the dynamic prediction of tile flow and soil moisture at catchment scales needs to account for
766 (1) the amount of drainable soil water that can be affected by the development of a capillary fringe
767 and (2) fluctuations in saturated storage ~~the groundwater water table~~, in addition to (3) the typical

768 ~~saturated storage near the tile pipe depth, (3) water table elevation above the tile pipe~~ and (4) the
769 soil saturated hydraulic conductivity considered by the steady-state flow Hooghoudt's equation.
770 The ~~saturated storage groundwater table~~ and matric potential changed dramatically between
771 seasons, affecting patterns of overall soil moisture and tile flow. Observations and model results
772 showed that low precipitation and higher evapotranspiration rates caused minimal tile flows during
773 the crop-growing season. Conversely, tile flow was often observed during the cold season, even
774 during small rainfall-runoff and snowmelt events, due to a seasonal increase in ~~the groundwater~~
775 ~~table and~~ soil-saturated storage.
776 Model sensitivity tests showed that the capillary fringe strongly affected the amount of drainable
777 soil water flowing into the tile. Tile flow increased with drainable water, but the relationship is
778 highly non-linear likely because, as the tile carrying capacity is exceeded more frequently, there is
779 more opportunity time for groundwater seepage and evapotranspiration. Finally, observations and
780 model results reveal a bimodal ~~soil~~-saturated storage response in the presence of tiles, which is
781 controlled by the relative positioning of the capillary fringe in relation to the soil surface and the
782 depth of tile drains below the soil surface. Capturing these dynamics is a critical advance enabling
783 the accurate prediction of the swift hydrological changes caused by the presence of tiles in models.
784 The TDM was developed as a first approximation from a single field site with the goal of providing
785 insight into control mechanisms of tile flow. Given this limitation, it is not yet widely applicable
786 across multiple field sites and for larger areas. ~~However~~Yet, the development of this module
787 provides critical insights into its potential and performance for hourly time-step simulations, as
788 well as the importance of ~~saturated storage regional groundwater table~~ fluctuations and simplifying
789 the capillary fringe parameters within models in some landscape types. Future work will-should
790 ~~include~~building on the current model ~~and~~ adapting it to ~~for~~ different soil textures, such as those in

791 clay loam soils, where preferential flow can have a strong impact on ~~soil-~~ssaturated storage and
792 tile flow. Also, explicit representation of unsaturated flow ~~will-~~may be needed to enable the use of
793 the model in regions where groundwater is disconnected from surface water, as commonly happens
794 in arid and semi-arid regions. Subsequent steps should include also the integration of the new TDM
795 model with CRHM's frozen soil and water quality modules.

796

797 **Code/Data availability**

798 The tile flow and soil water table data are not publicly available and will be provided upon request
799 to the data owner, Merrin Macrae. TDM code is not completely implemented in the main version
800 of the Cold Regions Hydrological Model platform and is provided ~~only-~~upon request to the
801 corresponding author.

802

803 **Author contribution**

804 MK and DC developed the new model code and performed the simulations. MM prepared the data
805 and supported the field work. JP developed CRHM. MK, DC and MM prepared the manuscript
806 with contributions from JP and RP. All authors edited the manuscript.

807

808 **Competing interests**

809 The contact author has declared that none of the authors has any competing interests.

810

811 **Acknowledgements**

812 Funding for this project was provided by the Canada First Excellence Research Fund's Global
813 Water Futures programme through its Agricultural Water Futures project. Funding for the
814 collection of the field data was provided by the Ontario Ministry of Agriculture, Food and Rural
815 Affairs. The support of the Biogeochemistry Lab at the University of Waterloo for the collection
816 of field data and of Tom Brown and Xing Fang of the Centre for Hydrology at the University of
817 Saskatchewan for CRHM development and updates is gratefully acknowledged. The Maitland
818 Valley Conservation Authority is thanked for providing some precipitation, rainfall, and
819 temperature data.

820

821 **References**

822 Akis R.: Simulation of Tile Drain Flows in an Alluvial Clayey Soil Using HYDRUS 1D,
823 American-Eurasian J. Agric. & Environ. Sci., 16 (4), 801-813,
824 <https://doi.org/10.5829/idosi.aejaes.2016.16.4.12906> , 2016.

825

826 Arheimer, B., Nilsson, J., and Lindstrom, G.: Experimenting with Coupled Hydro-Ecological
827 Models to Explore Measure Plans and Water Quality Goals in a Semi-Enclosed Swedish Bay,
828 Water, 7(7), 3906-3924, <https://doi.org/10.3390/w7073906>, 2015.

829

830 Arnold, J. G., Srinivasan, R., Muttiah, R. S., and Williams, J. R.: Large area hydrologic modeling
831 and assessment part I: model development, J. Am. Water. Resour. Assoc., 34, 73-89,
832 <https://doi.org/10.1111/j.1752-1688.1998.tb05961.x>, 1998.

833

834 Badr, A. W.: Physical properties of some North Carolina Organic Soils and the effect of land
835 development on these properties, M.S. Thesis, Department of Biological and Agricultural
836 Engineering, North Carolina State University, Raleigh, NC. 67 p., 1978.

837

838 Blear, W. (2nd Edition): Soil and Environmental Chemistry, Academic Press, eBook ISBN:
839 9780128041956, 2017.

840

841 ~~[Bouwer, H. and van Schilfgaarde, J.: Simplified method of predicting the fall of water table in](#)~~
842 ~~[drained land, Trans. ASAE. 6\(4\), 288-291, 296, 1963.](#)~~

843

844 Brockley, R. P.: The effect of nutrient and moisture on soil nutrient availability, nutrient uptake,
845 tissue nutrient concentration, and growth of Douglas-Fir seedlings, Master Thesis, The University
846 of British Columbia, 1976.

847

848 Broughton, R. and Jutras, P.: Farm Drainage. In the Canadian Encyclopedia,
849 <https://www.thecanadianencyclopedia.ca/en/article/farm-drainage/>, last access: 14 February 2019,
850 [2013](#).

851

852 [Clark, M. P., Nijssen, B., Lundquist, J. D., Kavetski, D., Rupp, D. E., Woods, R. A., Freer, J. E.,](#)
853 [Gutmann, E. D., Wood, A. W., Brekke, L. D., Arnold, J. R., Gochis, D. J., & Rasmussen, R. M.](#)
854 [A unified approach for process-based hydrologic modeling: 1. Modeling concept. Water Resources](#)
855 [Research, 51\(4\), 2498–2514. https://doi.org/https://doi.org/10.1002/2015WR017198, 2015a.](#)

856

857 [Clark, M. P., Nijssen, B., Lundquist, J. D., Kavetski, D., Rupp, D. E., Woods, R. A., Freer, J. E.,](#)
858 [Gutmann, E. D., Wood, A. W., Gochis, D. J., Rasmussen, R. M., Tarboton, D. G., Mahat, V.,](#)
859 [Flerchinger, G. N., & Marks, D. G. A unified approach for process-based hydrologic modeling: 2.](#)
860 [Model implementation and case studies. *Water Resources Research*, 51\(4\), 2515–2542.](#)
861 <https://doi.org/https://doi.org/10.1002/2015WR017200>, 2015b.

862
863 Coelho, B. B., Murray, R., Lapen, D., Topp, E., and Bruin, A.: Phosphorus and sediment loading
864 to surface waters from liquid swine manure application under different drainage and tillage
865 practices, *Agric. Water Manag.*, 104, 51-61, <https://doi.org/10.1016/j.agwat.2011.10.020>, 2012.

866
867 Cordeiro, M. R. C. and Ranjan, R. S.: Corn yield response to drainage and subirrigation in the
868 Canadian Prairies, *Trans. ASABE*. 55(5), 1771-1780, <https://doi.org/10.13031/2013.42369>, 2012.

869
870 Cordeiro, M. R. C., Wilson, H. F., Vanrobaeys, J., Pomeroy, J. W., Fang, X., and The Red-
871 Assiniboine Project Biophysical Modeling Team: Simulating cold-region hydrology in an
872 intensively drained agricultural watershed in Manitoba, Canada, using the Cold Region
873 Hydrological Model, *Hydrol. Earth Syst. Sci.*, 21, 3483-3506, [https://doi.org/10.5194/hess-21-](https://doi.org/10.5194/hess-21-3483-2017)
874 [3483-2017](https://doi.org/10.5194/hess-21-3483-2017), 2017.

875
876 Correll, D.: The role of phosphorus in the eutrophication of receiving waters: a review, *J. Environ.*
877 *Qual.*, 27, 261-266, <https://doi.org/10.2134/jeq1998.00472425002700020004x>, 1998.

878

879 [Costa, D., Klenk, K., Knoben, W., Ireson, A., Spiteri, R. J., and Clark, M.: OpenWQ v.1: A multi-](#)
880 [chemistry modelling framework to enable flexible, transparent, interoperable, and reproducible](#)
881 [water quality simulations in existing hydro-models, EGUsphere \[preprint\],](#)
882 <https://doi.org/10.5194/egusphere-2023-2787>, 2023.~~Costa, D., Klenk, K., Knoben, W., Ireson, A.,~~
883 ~~Spiteri, R., Clark, M.: A multi-chemistry modelling framework to enable flexible and reproducible~~
884 ~~water quality simulations in existing hydro-models: 1. The OpenWQ concept and the water quality~~
885 ~~modelling lab. ESS Open Archive.~~
886 <https://essopenarchive.org/doi/full/10.22541/essoar.168718167.75677635/v1>, 2023

887
888
889 ~~Costa, D., Klenk, K., Knoben, W.J.M., Ireson, A., Spiteri, R.J., Clark, M.P.: A multi-chemistry~~
890 ~~modelling framework to enable flexible and reproducible water quality simulations in existing~~
891 ~~hydro-models: 2. The OpenWQ SUMMA and OpenWQ CRHM model implementations and~~
892 ~~testing. ESS Open Archive. DOI:10.22541/essoar.168652285.59958331/v1, 2023.~~

893
894 Costa, D., Sutter, D., Shepherd, A., Jarvie, H., Wilson, H., Elliott, J., Liu, J., and Macrae, M.:
895 Impact of climate change on catchment nutrient dynamics: insights from around the
896 world. Environmental Reviews. **31**(1): 4-25. <https://doi.org/10.1139/er-2021-0109>, 2022

897
898 Costa, D., Baulch, H., Elliott, J., Pomeroy, J., and Wheater, H.: Modelling nutrient dynamics in
899 cold agricultural catchments: A review, Environ. Model. Softw., 124, 104586,
900 <https://doi.org/10.1016/j.envsoft.2019.104586>, 2020a.

901

902 Costa, D., Shook, K., Spence, C., Elliott, J., Baulch, H., Wilson, H., and Pomeroy, J.: Predicting
903 variable contributing areas, hydrological connectivity, and solute transport pathways for a
904 Canadian Prairie basin, *Water Resour. Res.*, 56, 1-23, <https://doi.org/10.1029/2020WR02798>,
905 2020b.

906
907 Costa, D., Burlando, P., Liong, S.-Y.: Coupling spatially distributed river and groundwater
908 transport models to investigate contaminant dynamics at river corridor scales. *Environmental*
909 *Modelling & Software*, 86, 91–110. <https://doi.org/10.1016/j.envsoft.2016.09.009>, 2016.

910
911 Costa, D., Pomeroy, J. W., Brown, T., Baulch, H., Elliott, J., and Macrae, M.: Advances in the
912 simulation of nutrient dynamics in cold climate agricultural basins: Developing new nitrogen and
913 phosphorus modules for the Cold Regions Hydrological Modelling Platform, *J. Hydrol.*, 603, 1-
914 17, <https://doi.org/10.1016/j.jhydrol.2021.126901>, 2021.

915
916 ~~Clark, M. P., Nijssen, B., Lundquist, J. D., Kavetski, D., Rupp, D. E., Woods, R. A., Freer, J. E.,~~
917 ~~Gutmann, E. D., Wood, A. W., Brekke, L. D., Arnold, J. R., Gochis, D. J., & Rasmussen, R. M.~~
918 ~~(2015). A unified approach for process-based hydrologic modeling: 1. Modeling concept. *Water*~~
919 ~~*Resources Research*, 51(4), 2498–2514.~~

920
921 ~~Clark, M. P., Nijssen, B., Lundquist, J. D., Kavetski, D., Rupp, D. E., Woods, R. A., Freer, J. E.,~~
922 ~~Gutmann, E. D., Wood, A. W., Gochis, D. J., Rasmussen, R. M., Tarboton, D. G., Mahat, V.,~~
923 ~~Flerchinger, G. N., & Marks, D. G. (2015). A unified approach for process-based hydrologic~~

924 ~~modeling: 2. Model implementation and case studies. *Water Resources Research*, 51(4), 2515–~~
925 ~~2542. [https://doi.org/https://doi.org/10.1002/2015WR017200](https://doi.org/10.1002/2015WR017200)~~

926

927 De Ridder, N. A., Takes, C. A. P., van Someren, C. L., Bos, M. G., Messemaeckers van de Graaff,
928 R. H., Bokkers, A. H. J., Stransky, J., Wiersma-Roche, M. F. L., and Beekman, T.: Drainage
929 Principles and Applications. International Institute for Lan Reclamation and Improvement, P.O.
930 Box 45 Wageningen The Netherlands, 1974.

931

932 Du, B., Arnold, J. G., Saleh, A., and Jaynes, D. B.: Development and application of SWAT to
933 landscapes with tiles and potholes, *Trans. ASAE*, 48, 1121-1133,
934 <https://doi.org/10.13031/2013.18522>, 2005.

935

936 Du, B., Saleh, A., Jaynes, D. B., and Arnold, J. G.: Evaluation of SWAT in simulating nitrate
937 nitrogen and atrazine fates in a watershed with tiles and potholes, *Trans. ASABE*, 49, 949-959,
938 <https://doi.org/10.13031/2013.21746>, 2006.

939

940 ECCC, Canadian Climate Normals 1981-2010 Station Data,
941 [https://climate.weather.gc.ca/climate_normals/results_1981_2010_e.html?searchType=stnProx&](https://climate.weather.gc.ca/climate_normals/results_1981_2010_e.html?searchType=stnProx&txtRadius=25&selCity=&selPark=&optProxType=custom&txtCentralLatDeg=43&txtCentralLatMin=41&txtCentralLatSec=55&txtCentralLongDeg=81&txtCentralLongMin=28&txtCentralLongSec=47&txtLatDecDeg=&txtLongDecDeg=&stnID=4545&dispBack=0)
942 [txtRadius=25&selCity=&selPark=&optProxType=custom&txtCentralLatDeg=43&txtCentralLat](https://climate.weather.gc.ca/climate_normals/results_1981_2010_e.html?searchType=stnProx&txtRadius=25&selCity=&selPark=&optProxType=custom&txtCentralLatDeg=43&txtCentralLatMin=41&txtCentralLatSec=55&txtCentralLongDeg=81&txtCentralLongMin=28&txtCentralLongSec=47&txtLatDecDeg=&txtLongDecDeg=&stnID=4545&dispBack=0)
943 [Min=41&txtCentralLatSec=55&txtCentralLongDeg=81&txtCentralLongMin=28&txtCentralLon](https://climate.weather.gc.ca/climate_normals/results_1981_2010_e.html?searchType=stnProx&txtRadius=25&selCity=&selPark=&optProxType=custom&txtCentralLatDeg=43&txtCentralLatMin=41&txtCentralLatSec=55&txtCentralLongDeg=81&txtCentralLongMin=28&txtCentralLongSec=47&txtLatDecDeg=&txtLongDecDeg=&stnID=4545&dispBack=0)
944 [gSec=47&txtLatDecDeg=&txtLongDecDeg=&stnID=4545&dispBack=0](https://climate.weather.gc.ca/climate_normals/results_1981_2010_e.html?searchType=stnProx&txtRadius=25&selCity=&selPark=&optProxType=custom&txtCentralLatDeg=43&txtCentralLatMin=41&txtCentralLatSec=55&txtCentralLongDeg=81&txtCentralLongMin=28&txtCentralLongSec=47&txtLatDecDeg=&txtLongDecDeg=&stnID=4545&dispBack=0), last access: 5 February
945 2020.

946

947 ~~Eckersten, H., Jansson, P. E., and Johnsson, H. (2nd edition): SOILN model user's manual,~~
948 ~~Division of Agricultural Hydrotechnics Communications 94:4, Department of soil Sciences,~~
949 ~~Swedish University of Agricultural Sciences, 58pp, Uppsala, 1994.~~

950

951 Environment Canada, Canadian Climate Normals 1981-2010 Station Data,
952 https://climate.weather.gc.ca/climate_data/daily_data_e.html?hlyRange=%7C&dlyRange=1966-06-01%7C2021-06-14&mlyRange=1966-01-01%7C2006-12-01&StationID=4603&Prov=ON&urlExtension=_e.html&searchType=stnName&optLimit=yearRange&StartYear=1840&EndYear=2022&selRowPerPage=25&Line=0&searchMethod=contains&Month=6&Day=4&txtStationName=Wroxeter&timeframe=2&Year=2021, last access: 10
957 May 2020.

958

959 Fang, X., Pomeroy, J. W., Westbrook, C. J., Guo, X., Minke, A. G., and Brown, T.: Prediction of
960 snowmelt derived streamflow in a wetland dominated prairie basin, Hydrol. Earth Syst. Sci., 14,
961 991-1006, <https://doi.org/10.5194/hess-14-991-2010>, 2010.

962

963 Fang, X., Pomeroy, J. W., Ellis, C. R., MacDonald, M. K., DeBeer, C. M., and Brown, T.: Multi-
964 variable evaluation of hydrological model predictions for a headwater basin in the Canadian Rocky
965 Mountains, Hydrol. Earth Syst. Sci., 17, 1635-1659, <https://doi.org/10.5194/hess-17-1635-2013>,
966 2013.

967

968 Filippelli, G. M.: The global phosphorus cycle, Rev. Mineral. and Geochem., 48, 391-425,
969 <https://doi.org/10.2138/rmg.2002.48.10>, 2002.

970
971 Frey, S. K., Hwang, H. T., Park, Y. J., Hussain, S. I., Gottschall, N., Edwards, M., and Lapen, D.
972 R.: Dual permeability modeling of tile drain management influences on hydrologic and nutrient
973 transport characteristics in macroporous soil, *J. Hydrol.*, 535, 392-406,
974 <http://dx.doi.org/10.1016/j.jhydrol.2016.01.073>, 2016.

975
976 Gentry, L. E., David, M. B., Royer, T. V., Mitchell, C. A., and Starks, K.: Phosphorus transport
977 pathways to streams in tile-drained agricultural watersheds, *J. Environ. Quality.*, 36, 408-415,
978 <https://doi.org/10.2134/jeq2006.0098>, 2007.

979
980 Garcia-Gutierrez, C., Pachepsky, Y., and Martin, M. A.: Technical note: Saturated hydraulic
981 conductivity and textural heterogeneity of soils, *Hydrol. Earth Syst. Sci.*, 22, 3923-3932,
982 <https://doi.org/10.5194/hess-22-3923-2018>, 2018.

983
984 Green, C. H., Tomer, M. D., Di Luzio, M., and Arnold, J. G.: Hydrologic evaluation of the Soil
985 and Water Assessment Tool for large tile-drained watershed in Iowa, *Trans. ASABE.*, 49, 413-
986 422, <https://doi.org/10.13031/2013.20415>, 2006.

987
988 Hansen, A. L., Jakobsen, R., Refsgaard, J. C., Hojberg, A. L., Iversen, B. V., and Kjaergaard, C.:
989 Groundwater dynamics and effect of tile drainage on water flow across the redox interface in a
990 Danish Weichsel till area, *Advances in Water Resources*, 123, 23-39,
991 <https://doi.org/10.1016/j.advwatres.2018.10.022>, 2019.

992

993 Hirt, U., Wetzig, A., Amatya, M. D., and Matranga, M.: Impact of seasonality on artificial drainage
994 discharge under temperate climate conditions, *Int. Rev. Hydrobiol.*, 96, 561-577,
995 <https://doi.org/10.1002/iroh.201111274>, 2011.

996

997 Hooghoudt, S. B.: Bijdrage tot de kennis van enige natuurkundige grootheden van de grond.
998 Verslagen van Landbouwkundige Onderzoekingen, 46(7), 515-707, the Hague, The Netherlands
999 (in Dutch), 1940.

1000

1001 ICID: World Drained Area-2018. International Commission on Irrigation and Drainage.
1002 <http://www.icid.org/world-drained-area.pdf> , last access: 14 February 2019.

1003

1004 Jamieson, A., Madramootoo, C. A., and Enright, P.: Phosphorus losses in surface and subsurface
1005 runoff from a snowmelt event on an agricultural field in Quebec, *Can. Biosyst. Eng.*, 45, 11-17,
1006 2003.

1007

1008 Jarvie, H. P., Johnson, L. T., Sharpley, A. N., Smith, D. R., Baker, D. B., Bruulsema, T. W., and
1009 Confesor, R.: Increased Soluble Phosphorus Loads to Lake Erie: Unintended Consequences of
1010 Conservation Practices?, *J. Environ. Qual.*, 46, 123-132, <https://doi.org/10.2134/jeq2016.07.0248>,
1011 2017.

1012

1013 Javani-Jouni, H., Liaghat, A., Hassanoghli, A., and Henk, R.: Managing controlled drainage in
1014 irrigated farmers' fields: A case study in the Moghan Plain, Iran, *Agric. Water Manag.*, 208, 393-
1015 405, <https://doi.org/10.1016/j.agwat.2018.06.037>, 2018.

1016
1017 Johnsen, K. E., Liu, H. H., Dane, J. H., Ahuja, L. R., and Workman, S. R.: Simulating Fluctuating
1018 Water Tables and Tile Drainage with a Modified Root Zone Water Quality Model and a New
1019 Model WAFLOWM, Transactions of the ASAE, 38 (1), 75-83,
1020 <https://doi.org/10.10031/2013.27814>, 1995.

1021
1022 Kiesel, J., Fohrer, N., Schmalz, B., and White, M. J.: Incorporating landscape depressions and tile
1023 drainages of a northern German lowland catchment into a semi-distributed model, Hydrol.
1024 Process., 24, 1472-1486, <https://doi.org/10.1002/hyp.7607>, 2010.

1025
1026 King, K. W., Williams, M. R., Macrae, M. L., Fausey, N. R., Frankenberger, J., Smith, D. R.,
1027 Kleinman, P. A. J., and Brown, L. C.: Phosphorus transport in agricultural subsurface drainage: A
1028 review, J. Environ. Qual., 44(2), 467-485, <https://doi.org/10.2134/jeq2014.04.0163>, 2015.

1029
1030 King, K. W., Williams, M. R., and Fausey, N. R.: Effect of crop type and season on nutrient
1031 leaching to tile drainage under a corn-soybean rotation, J. Soil and Water Conserv., 71, 56-68,
1032 <https://doi.org/10.2489/jswc.71.1.56>, 2016.

1033
1034 ~~Kirkham, D.: Theory of land drainage, in, Drainage of Agricultural Lands. Agronomy Monograph,~~
1035 ~~No. 7, American Society of Agronomy, Madison, Wisconsin, 1957.~~

1036

1037 Kladivko, E. J., Grochulska, J., Turco, R. F., Van Scoyoc, G. E., and Eigel, J. D.: Pesticide and
1038 nitrate transport into subsurface tile drains of different spacings, *J. Environ. Qual.*, 28, 997-1004,
1039 <https://doi.org/10.2134/jeq1999.00472425002800030033x>, 1999.

1040

1041 Klaiber, L. B., Kramer, S. R., and Young, E. O.: Impacts of Tile Drainage on Phosphorus Losses
1042 from Edge-of-field Plots in the Lake Champlain Basin of New York, *Water*, 12, 328,
1043 <https://doi.org/10.3390/w12020328>, 2020.

1044

1045 ~~Koek~~Koch, S., Bauwe, A., and Lennartz, B.: Application of SWAT Model for a Tile-Drained
1046 Lowland Catchment in North-Eastern Germany on Subbasin Scale, *Water Resour. Manage.*, 27,
1047 791-805, <https://doi.org/10.1007/s11269-012-0215-x>, 2013.

1048

1049 Kokulan, V.: Environmental and Economic Consequences of Tile Drainage Systems in Canada,
1050 The Canadian Agri-Food Policy Institute (CAPI), 2019.

1051

1052 Kokulan, V., Macrae, M. L., Ali, G. A., and Lobb, D. A.: Hydroclimatic controls on runoff
1053 activation in a artificially drained, near-level vertisolic clay landscape in a Prairie climate, *Hyrol.*
1054 *Process.*, 33, 602-615, <https://doi.org/10.1002/hyp.13347>, 2019a.

1055

1056 Lam, W. V., Macrae, M. L., English, M. C., O'Halloran, I. P., Plach, J. M., and Wang, Y.: Seasonal
1057 and event-based drives of runoff and phosphorus export through agricultural tile drains under
1058 sandy loam soil in a cool temperate region, *Hydro. Process.*, 30, 2644-2656,
1059 <https://doi.org/10.1002/hyp.10871>, 2016a.

1060
1061 Lam, W. V., Macrae, M. L., English, M. C., O'Halloran, I., and Wang, Y.: Effects of tillage
1062 practices on phosphorus transport in tile drain effluent in sandy loam agricultural soils in Ontario,
1063 Canada, *J. Great Lakes Res.*, 42(6), 1260-1270, <https://dx.doi.org/10.1016/j.jglr.2015.12.015>,
1064 2016b.

1065
1066 ~~Larsbo, M., and Jarvis, N.: MACRO 5.0. A model of water flow and solute transport in~~
1067 ~~microporous soil, Technical description. Swedish University of Agricultural Sciences, Division of~~
1068 ~~Environmental Physics, Emergo 2003:6 Report, ISSN 1651-7210, ISBN 91-576-6592-3, 2003.~~

1069
1070 Lindstrom, G., Pers, C., Rosberg, J., Stromqvist, J., and Arheimer, B.: Development and testing of
1071 the HYPE (Hydrological Predictions for the Environment) water quality model for different scales,
1072 *Hydrol. Res.*, 41(3-4), 295-319, <https://doi.org/10.2166/nh.2010.007>, 2010.

1073
1074 Logsdon, S. D., Schilling, K. E., Hernandez-Ramirez, G., Prueger, J. H., Hatfield, J. L., and Sauer,
1075 T. J.: Field estimation of specific yield in a central Iowa crop field, *Hydrol. Process.*, 24, 1369-
1076 1377, <https://doi.org/10.1002/hyp.7600>, 2010.

1077
1078 Macrae, M. L., English, M. C., Schiff, S. L., and Stone, M. L.: Intra-annual variability in the
1079 contribution of tile drains to basin discharge and phosphorus export in a first order agricultural
1080 catchment, *Agric. Water Manag.*, 92, 171-182, <https://doi.org/10.1016/j.agwat.2007.05.015>, 2007.

1081

1082 Macrae, M. L., Ali, G. A., King, K. W., Plach, J. M., Puer, W. T., Williams, M., Morison, M. Q.,
1083 and Tang, W.: Evaluating Hydrologic Response in Tile-Drained Landscapes: Implications for
1084 Phosphorus Transport, *J. Environ. Qual.*, 48(5), 1347-1355,
1085 <https://doi.org/10.2134/jeq2019.02.0060>, 2019.

1086

1087 Malzone, J. M., Lowry, C. S., and Ward, A. S.: Response of the hyporheic zone to transient
1088 groundwater fluctuations on the annual and storm event time scales, *Water Resour. Res.*, 52, 5301-
1089 5321, <https://doi.org/10.1002/2015WR018056>, 2016.

1090

1091 Mizukami, N., Clark, M. P., Sampson, K., Nijssen, B., Mao, Y., McMillan, H., Viger, R. J.,
1092 Markstrom, S. L., Hay, L. E., Woods, R., Arnold, J. R., & Brekke, L. D. ~~(2016)~~. mizuRoute version
1093 1: A river network routing tool for a continental domain water resources applications.
1094 *Geoscientific Model Development*, 9, 2223–2238. <https://doi.org/10.5194/gmd-9-2223-2016> ,
1095 [2016](https://doi.org/10.5194/gmd-9-2223-2016).

1096

1097 Moriasi, D. N., Arnold, J. G., Van Liew, M. W., Bingner, R. L., Harmel, R. D., and Veith, T. L.:
1098 Model Evaluation Guidelines for Systematic Quantification of Accuracy in Watershed
1099 Simulations, *Trans. ASABE*, 50(3), 885-900, <https://doi.org/10.13031/2013.23153>, 2007.

1100

1101 Moriasi, D. N., Gowda, P. H., Arnold, J. G., Mulla, D. J., Ale, S., Steiner, J. L., and Tomer, M. D.:
1102 Evaluation of the Hooghoudt and Kirkham Tile Drain Equations in the Soil and Water Assessment
1103 Tool to Simulate Tile Flow and Nitrate-Nitrogen, *J. Environ. Qual.*, 42, 1699-1710,
1104 <https://doi.org/10.2134/jeq2013.01.0018>, 2013.

1105

1106 [OMAFRA: Tile Drainage Area, Government of Ontario, Canada, available at](https://geohub.lio.gov.on.ca/datasets/ontariocal11::tile-drainage-area/explore?showTable=true)

1107 <https://geohub.lio.gov.on.ca/datasets/ontariocal11::tile-drainage-area/explore?showTable=true>,

1108 [2023.](#)

1109

1110 Plach, J. M., Macrae, M. L., Ali, G. A., Brunke, R. R., English, M. C., Ferguson, G., Lam, W. V.,

1111 Lozier, T. M., McKague, K., O'Halloran, I. P., Opolko, G., and Van Esbroeck, C. J.: Supply and

1112 Transport Limitations on Phosphorus Losses from Agricultural Fields in the Lower Great Lakes

1113 Region, Canada, J. Environ. Qual., 47, 96-105, <https://doi.org/10.2134/jeq2017.06.0234>, 2018a.

1114

1115 Plach, J. M., Macrae, M. L., Williams, M. R., Lee, B. D., and King, K. W.: Dominant glacial

1116 landforms of the lower Great Lakes region exhibit different soil phosphorus chemistry and

1117 potential risk for phosphorus loss, J. Great Lakes Res., 44, 1057-1067,

1118 <https://doi.org/10/1016/j.jglr.2018.07.005>, 2018b.

1119

1120 Plach, J., Puer, W., Macrae, M., Kompanizare, M., McKague, K., Carlow, R., and Brunke, R.:

1121 Agricultural Edge of Field Phosphorus Losses in Ontario, Canada: Importance of the Nongrowing

1122 Season in Cold Regions, J. Environ. Qual., 48, 813-821, <https://doi.org/10.2134/jeq2018.11.0418>,

1123 2019.

1124

1125 Puer, W. T., Macrae, M., Buckley, A., and Reid, K.: Contribution of preferential flow to tile

1126 drainage varies spatially and temporally, Vadose Zone J., 19: e20043,

1127 <https://doi.org/10.1002/vzj2.20043>, 2020.

1128

1129 Pomeroy, J. W., Gray, D. M., Shook, K. R., Toth, B., Essery, R. L. H., Pietroniro, A., and
1130 Hedstrom, N. R.: An evaluation of snow accumulation and ablation processes for land surface
1131 modelling, *Hydrol. Process.*, 12, 2339-2367, [https://doi.org/10.1002/\(SICI\)1099-](https://doi.org/10.1002/(SICI)1099-1085(199812)12:15)
1132 [1085\(199812\)12:15](https://doi.org/10.1002/(SICI)1099-1085(199812)12:15), 1998.

1133

1134 Pomeroy, J. W., Gray, D. M., Brown, T., Hedstrom, N. R., Quinton, W. L., Granger, R. J., and
1135 Carey, S. K.: The cold regions hydrological model: a platform for basing process representation
1136 and model structure on physical evidence, *Hydrol. Process.*, 21, 2650-2667,
1137 <https://doi.org/10.1002/hyp.6787>, 2007.

1138

1139 Pomeroy, J. W., Fang, X., Shook, K., and Whitfield, P. H.: Predicting in Ungauged Basins Using
1140 Physical Principles Obtained Using the Deductive, Inductive, and Abductive Reasoning Approach,
1141 https://research-groups.usask.ca/hydrology/documents/pubs/papers/pomeroy_et_al_2003_3.pdf ,
1142 2013.

1143

1144 Pomeroy, J. W., Fang, X., and Marks, D. G.: The cold rain-on-snow event of June 2013 in the
1145 Canadian Rockies - characteristics and diagnosis, *Hydrol. Process.*, 30, 2899-2914,
1146 <https://doi.org/10.1002/hyp.10905>, 2016.

1147

1148 Pomeroy, J. W., Brown, T., Fang, X., Shook, K. R., Pradhananga, D., Armstrong, R., Harder, P.,
1149 Marsh, C., Costa, D., Krogh, S. A., Aubry-Wake, C., Annand, H., Lawford, P., He, Z.,
1150 Kompanizare, M., and Lopez Moreno, J. I.: The cold regions hydrological modelling platform for

1151 hydrological diagnosis and prediction based on process understanding, *J. of Hydrol.*, 615 (A),
1152 128711, <https://doi.org/10.1016/j.jhydrol.2022.128711>, 2022.

1153

1154 Qi, P., Zhang, G., Xu, Y. J., Wang, L., Ding, C., and Cheng, C.: Assessing the Influence of
1155 Precipitation on Shallow Groundwater Table Response Using Combination of Singular Value
1156 Decomposition and Cross-Wavelet Approaches, *Water*, 10, 598,
1157 <https://doi.org/10.3390/w10050598>, 2018.

1158

1159 Quinton, J. G., Govers, G., van Oost, K., and Bardgett, R.: The impact of agricultural soil erosion
1160 on biochemical cycling, *Nat. Geosci.*, 3, 311-314, <https://doi.org/10.1038/ngeo838>, 2010.

1161

1162 Raats, P. A. C. and Gardner, W. R.: Movement of water in saturated zone near a water table. Ch.
1163 13 in *Drainage for agriculture*, J. van Schilfgraade, Ed., Agronomy Monograph. No. 17, American
1164 Society of Agronomy, Madison, WI, pp. 331-357, 1974.

1165

1166 Radcliffe, D. E., Reid, D. K., Blomback, K., Bolster, C. H., Collick, A. S., Easton, Z. M.,
1167 Francesconi, W., Fuka, D. R., Johnsson, H., King, K., Larsbo, M., Youssef, M. A., Mulkey, A. S.,
1168 Nelson, N. O., Persson, K., Ramirez-Avila, J. J., Schmieder, F., and Smith, D. R.: Applicability of
1169 Models to Predict Phosphorus Losses in Drained Fields: A Review, *J. Environ. Qual.*, 44, 614-
1170 628, <https://doi.org/10.2134/jeq2014.05.0220>, 2015.

1171

1172 Rahman, M. M., Lin, Z., Jia, X., Steele, D. D., and DeSutter, T. M.: Impact of subsurface drainage
1173 on streamflows in Red River of the North basin, *J. Hydrol.*, 511, 474-483,
1174 <https://doi.org/10.1016/j.jhydrol.2014.01.070>, 2014.

1175

1176 Refsgaard, J. C. and Storm, B.: MIKE SHE. In: Singh VP (ed) Computer models of watershed
1177 hydrology, Highlands Ranch, Water Research Pub, Colorado, 1995.

1178

1179 Richards L. A.: Capillary conduction of liquids through porous medium, *Physics*, 1 (5): 318-333,
1180 Bibcode:1931Physi...1..318R. <https://doi.org/10.1063/1.1745010>, 1931.

1181

1182 Rozemeijer, J. C., Visser, A., Borren, W., Winegram, M., van der Velde, Y., Klein, J., and Broers,
1183 H. P.: High-frequency monitoring of water fluxes and nutrient loads to assess the effects of
1184 controlled drainage on water storage and nutrient transport, *Hydrol. Earth Syst. Sci.*, 20, 347-358,
1185 <https://doi.org/10.5194/hess-20-347-2016>, 2016.

1186

1187 Rust, W., Holman, I., Bloomfield, J. Cuthbert, M., and Corstanje, R.: Understanding the potential
1188 of climate teleconnections to project future groundwater drought, *Hydrol. Earth Syst. Sci.*, 23,
1189 3233-3245, <https://doi.org/10.5194/hess-23-3233-2019>, 2019.

1190

1191 Ruttenger, K.: The global phosphorus cycle. In *Biochemistry*, Vol. 8, treatise on geochemistry,
1192 Schlesinger W (ed) (eds. H. Holland and K. Turekian). Elsevier-Pergamon: Oxford; 585-643,
1193 2005.

1194

1195 Searcy, J. and Hardison, C. H.: Double –Mass Curves. Manual of Hydrology: Part 1, General
1196 Surface-Water Techniques, Geological Survey Water-Supply Paper 1541-B, 1960.
1197

1198 Schindler, D. W.: Recent advances in the understanding and management of eutrophication,
1199 Limnol. Oceanogr., 51, 356-363, https://doi.org/10.4319/lo.2006.51.1_part_2.0356, 2006.
1200

1201 Sharpley, A. N., Hedley, M. J., Sibbesen, E., Hillbricht-Ilkowska, A., House, W. A., and
1202 Ryszowski, L.: Phosphorus transfer from terrestrial to aquatic ecosystems, In Phosphorus in the
1203 global environment, Tiessen H (ed), Scientific Committee on Problems of the Environment
1204 (SCOPE). John Wiley & SonsLtd.: Chichester; 171-199, 1995.

1205
1206

1207 Simunek J., van Genuchten M. Th., and Sejna M.: The HYDRUS Software Package for Simulating
1208 Two- and Three-Dimensional Movement of Water, Heat and Multiple Solutes in Variably-
1209 Saturated Media, Technical Manual, Version 2.0, PC Progress, Prague, Czech Republic, pp. 258,
1210 2011.
1211

1212 Skaggs, R. W.: A water management model for shallow water table soils, University of North
1213 Carolina, Water Resource Research Institute, Technical Report 134, 1978.
1214

1215 Skaggs, R. W.: Combination surface-subsurface drainage systems for humid regions. J. Irrig.
1216 Drain. Div., ASCE. 106(IR4), 265-283, 1980a.
1217

1218 Skaggs, R. W.: Drainmod Reference Report, Methods for Design and Evaluation of Drainage-
1219 Water Management Systems for Soils with High Water Tables, U.S. Department of Agriculture,
1220 Soil Conservation Service, North Carolina State University, Raleigh, North Carolina, 1980b.
1221
1222 Skaggs, R. W., Wells, L. G., and Ghate, S. R.: Predicted and measured drainable porosities for
1223 field soils, Trans. ASAE, 21(3), 522-528, https://uknowledge.uky.edu/bae_facpub/199, 1978.
1224
1225 Skaggs, R. W., Youssef, M. A., and Chescheir, G. M.: DRAINMOD: Model Use, Calibration, and
1226 Validation, Trans. ASABE, 55(4), 1509-1522, <https://doi.org/10.13031/2013.42259>, 2012.
1227
1228 Smedema, L. K., Vlotman, W. F., and Rycroft, D.: Modern land Drainage. Planning, design and
1229 management of agricultural drainage systems, London: Taylor & Francis.
1230 <https://doi.org/10.1201/9781003>, 2004.
1231
1232 Smith, D. R., King, K. W., Johnson, L., Francesconi, W., Richards, P., Baker, D., and Sharpley,
1233 A. N.: Surface runoff and tile drainage transport of phosphorus in the Midwestern United States,
1234 J. Environ. Qual., 44, 495-502, <https://doi.org/10.2134/jeq2014.04.0176>, 2015.
1235
1236 Tomer, M. D., Meek, D. W., Jaynes, D. B., and Hatfield, J. L.: Evaluation of nitrate nitrogen fluxes
1237 from a tile-drained watershed in Central Iowa, J. Environ. Qual., 32, 642-653,
1238 <https://doi.org/10.2134/jeq2003.6420>, 2003.
1239

1240 Twarakavi, N. K. C., Sakai, M., and Simunek, J.: An objective analysis of the dynamic nature of
1241 field capacity, *Water Resour. Res.*, 45, W10410, <https://doi.org/10.1029/2009WR007944>, 2009.
1242

1243 Van Esbroeck, C. J., Macrae, M. L., Brunke, R. I., and McKague, K.: Annual and seasonal
1244 phosphorus export in surface runoff and tile drainage from agricultural fields with cold temperate
1245 climates, *J. Great Lakes Res.*, 42(6), 1271-1280, <https://doi.org/10.1016/j.jglr.2015.12.014>, 2016.
1246

1247 Van Esbroeck, C. J., Macrae, M. L., Brunke, R. R., and McKague, K.: Surface and subsurface
1248 phosphorus export from agricultural fields during peak flow events over the nongrowing season in
1249 regions with cool, temperate climates, *Journal of Soil and Water Conservation*, 72(1), 65-76,
1250 <https://doi:10.2489/jswc.72.1.65> , 2017.
1251

1252 ~~Van Schilfgaarde, J.: Nonsteady flow to drains, In *Drainage for Agriculture*, J. van Schilfgaarde,~~
1253 ~~ed. American Society of Agronomy, Madison, WI. PP 245-270, 1974.~~
1254

1255 Vaughan, P. J., Suarez, D. L., Simunek, J., Corwin, D. L., and Rhoades, J. D.: Role of Groundwater
1256 Flow in Tile Drain Discharge, *J. Environ. Qual.*, 28, 403-410,
1257 <https://doi.org/10.2134/jeq1999.00472425002800020006x>, 1999.
1258

1259 Vidon, P. and Cuadra, P. E.: Impact of precipitation characteristics on soil hydrology in tile drained
1260 landscapes, *Hydrol. Process.*, 24, 1821-1833, <https://doi.org/10.1002/hyp.7627>, 2010.
1261

1262 Vivekananthan, K.: Environmental and Economic Consequences of Tile Drainage Systems in
1263 Canada, The Canadian Agri-Food Policy Institute, www.capi-icpa.ca, 2019.
1264

1265 Vivekananthan, K., Macrae, M., Lobb, D. A., and Ali, G. A.: Contribution of overland and tile
1266 flow to runoff and nutrient losses from vertisols in Manitoba, Canada, *J. Environ. Qual.*, 48(4),
1267 959-965, <https://doi.org/10.2134/jeq2019.03.0103>, 2019.
1268

1269 Waichler, S. R. and Wigmosta, M. S.: Development of Hourly Meteorological Values from Daily
1270 Data and Significance to Hydrological Modeling at H. J. Andrews Experimental Forest, *Am.*
1271 *Meteorol. Soc.*, 4, 251-263, [https://doi.org/10.1175/1525-
1272 7541\(2003\)4<251:DOHMFV>2.0.CO;2](https://doi.org/10.1175/1525-7541(2003)4<251:DOHMFV>2.0.CO;2), 2003.
1273

1274 Williams, M. R., King, K. W., and Fausey, N. R.: Drainage water management effects on tile
1275 discharge and water quality, *Agric. Water Manag.*, 148, 43-51,
1276 <http://dx.doi.org/10.1016/j.agwat.2014.09.017>, 2015.
1277

1278 Williams, M. R., King, K. W., Ford, W., Buda, A. R., and Kennedy, C. D.: Effect of tillage on
1279 macropore flow and phosphorus transport to tile drains, *Water Resour. Res.*, 52, 2868-2882,
1280 <https://doi.org/10.1002/2015WR017650>, 2016.
1281

1282 Williams, M. R., Livingston, S. J., Heathman, G. C., and McAfee, S. J.: Thresholds for run-off
1283 generation in a drained closed depression, *Hydrol. Process.*, 1-14,
1284 <https://doi.org/10.1002/hyp.13477>, 2019.

1285

1286 Youngs, E. G.: Effect of the Capillary fringe on Steady-State Water Tables in drained Lands, J.

1287 Irrig. Drain. Eng., 138(9), 809-814, [https://doi.org/10.1061/\(ASCE\)IR.1943-4774.0000467](https://doi.org/10.1061/(ASCE)IR.1943-4774.0000467), 2012.

1288

1289

1290 **Appendix A**

1291 Table A1. Instrument names and descriptions

Instrument name	Description
Hach Flo-tote and FL900 logger	Flow velocity and water level measurement
U20, Onset Ltd.	Barometrically-corrected pressure transducer
Temperature Smart Sensor S-THB-M002	Air temperature measurement
Wind Smart Sensor S-WSET-M002	Wind speed measurement
(Silicon Pyranometer)-S-LIB-M003	Solar radiation sensor
Tipping bucketrain gauge, 0.2 mm Rainfall Smart Sensor – SRGB-M002	Rainfall measurement
RH Smart Sensor(S-THB-M002)	Relative Humidity measurement

1292

1293

1294

1295 **Appendix B**

1296 Table B1. Parameter names and their symbols in CRHM platform

Parameter symbol	Parameter name
Tair	Air temperature

Wspeed	Wind speed
RH	Relative Humidity
Qsi	Incoming solar irradiance
R	Rainfall
WQ_soil	Water Quality soil module
WT	Water table elevation above the semipermeable layer
SSS	Soil saturated storage or the saturated part of the soil moisture
soil_moist	Soil moisture
Porosity_soil	Soil porosity
AL	Above layer
BL	Below layer
GWRDK_s	Groundwater level fluctuations, groundwater recharge and discharge Saturated hydraulic conductivity

1297

1298

1299

1300 **Appendix C**

1301

1302 Here, it was shown how seasonal factors ($f_{y,i}$) is assessed for different years. Equation (4) can be
 1303 written as:

1304

1305 $G_{y,i} = G \times f_{y,i}$ (C1)

1306

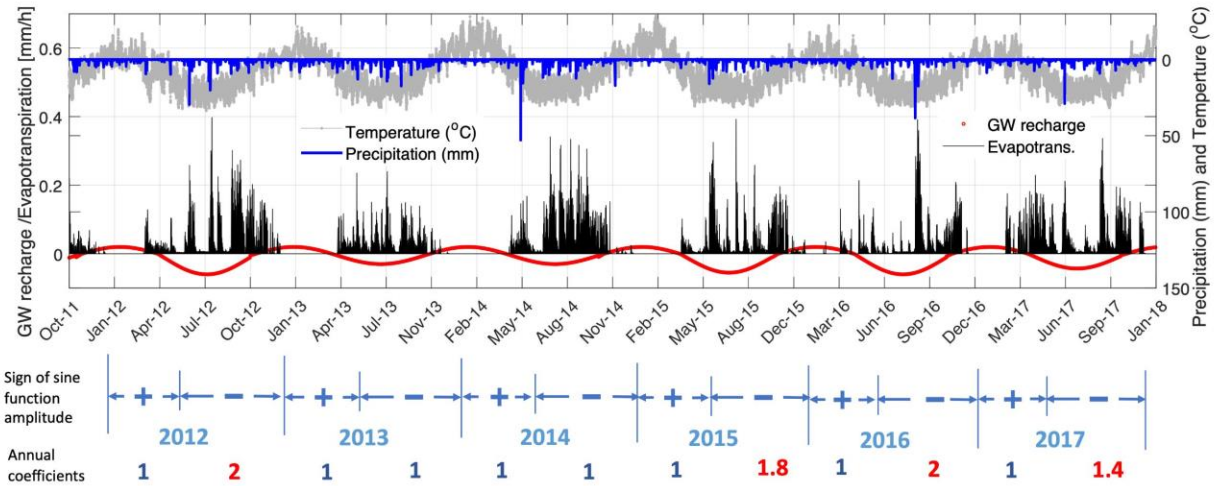
1307 For each year (y), $f_{y,i}$ for the first ($f_{y,1}$) and second ($f_{y,2}$) part of the sine function (G) were
 1308 assessed individually. It should be note that in first and second part of the sine function for each
 1309 year G is larger than zero ($G \geq 0$) and smaller than zero ($G < 0$), respectively. G can be defined
 1310 for the two parts as:

1311

$$1312 \begin{cases} \text{if } G \geq 0 [i = 1] \text{ then } f_{y,1} = x \\ \text{if } G < 0 [i = 2] \text{ then } f_{y,2} = y \end{cases} \quad (\text{C-2})$$

1313

1314 G is the sine function representing the annual fluctuations in water-table saturated storage
 1315 (WT/SSS) or it can be simply defined as the percolation rate (in mm hr^{-1}) of soil water to
 1316 groundwater through lower semi-permeable layer. So, for n years there are $n \times 2$ $f_{y,i}$ values. The
 1317 default values for $f_{y,i}$ are 1 and the default values can be changed for each year and for first and
 1318 second parts in each year independently. Calculated $G_{y,i}$ in each time step add or subtracted to or
 1319 from the total soil moisture depend on its sign. The $f_{y,i}$ values for the sine function parameters are
 1320 presented in Fig. C1. The verified sine function time series along with time series of temperature,
 1321 precipitation and calculated evapotranspiration are shown in Fig. C1. In this figure it is obvious
 1322 that in years 2012 and 2015 to 2017 the warm season amplitudes are larger. The ET values are
 1323 happened more in the warm seasons (growing seasons). Also, the seasonal oscillation in sine
 1324 function is very similar to the temperature general oscillations.



1325

1326 Figure C1. Time series of the adjustable sine function along with the time serieses of calculated evapotranspiration, temperature and
 1327 precipitation during the study period from Oct 2011 to Sept 2018.

1328

1329

1330 **Appendix D**

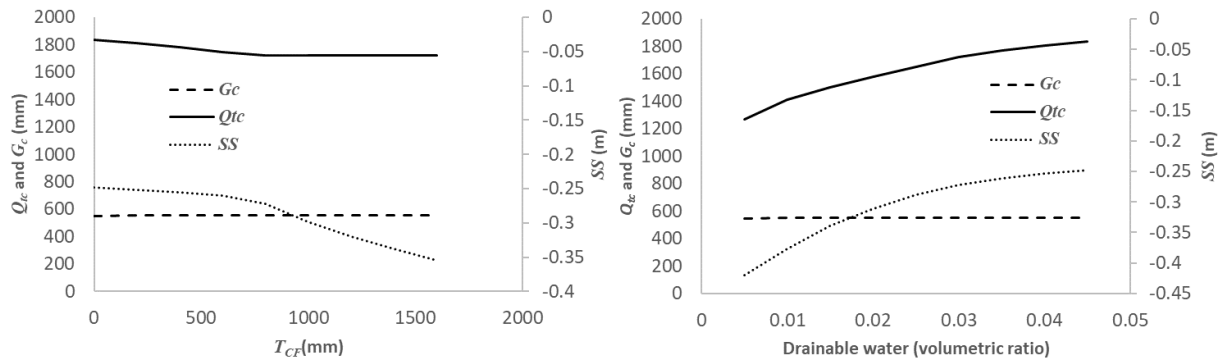
1331 A sensitivity analysis was conducted for the cumulative tile flow (Q_{tc}), mean soil [saturated storage](#)
 1332 [\(SS\)](#) (it is equal to water table elevation, WT_{m} , as it is mentioned in Eq. 3) and cumulative outflow
 1333 rate from the semi-permeable layer at the bottom of the soil to groundwater (G_c) (see section 2.4.5,
 1334 Eq. 4) with respect to six module parameters. Additionally, an approach for assessing model
 1335 parameters at a new sites, potentially lacking water table elevation and tile flow observations is
 1336 proposed.

1337

1338 **D.1 Sensitivity analysis**

1339 In this section, the sensitivity of Q_{tc} , SS and G_c to six distinct module parameters, namely capillary
 1340 fringe thickness (T_{CF}), capillary fringe drainable water (ϕ_c), soil saturated hydraulic conductivity
 1341 (K), soil thickness (T_{SL}), sine function amplitude (A) and sine function (B) was examined. Q_{tc} , G_c
 1342 and SS were computed over the entire simulation period, expressed in units of mm, mm and m,

1343 respectively. Figures D-1a to f illustrate these sensitivities, with each parameter's impact discussed
 1344 in dedicated sections.

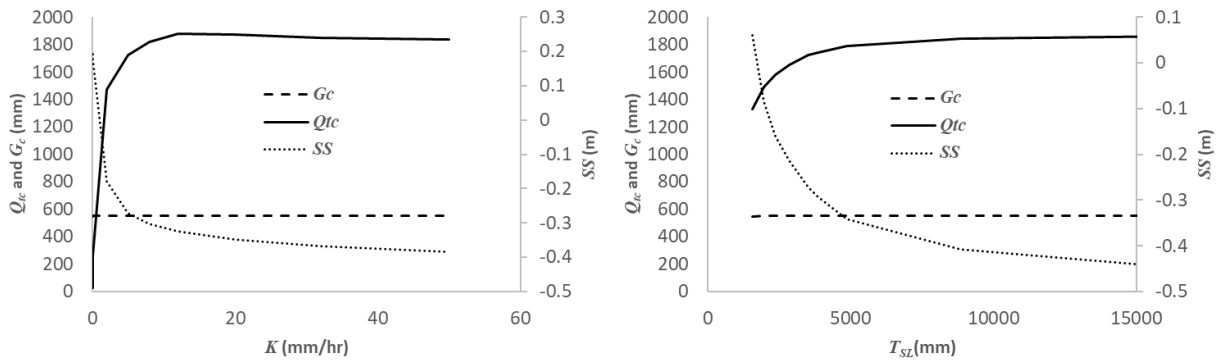


1345

1346

a)

b)

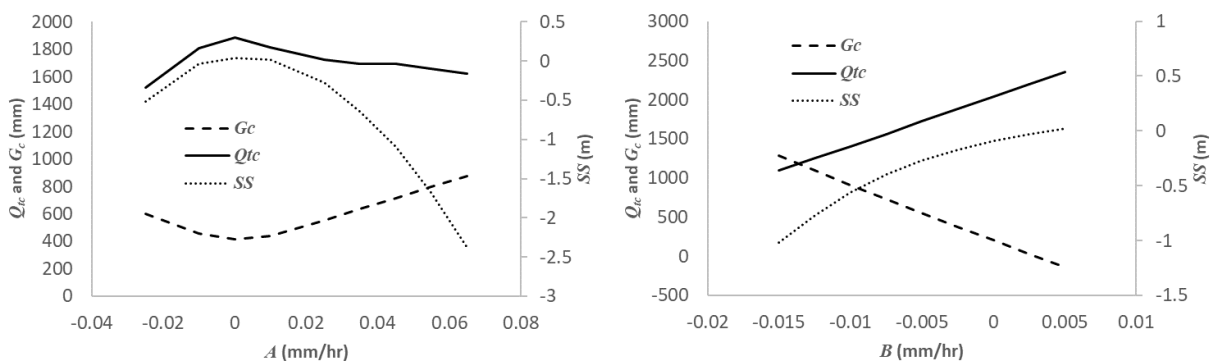


1347

1348

c)

d)



1349

1350

e)

f)

1351 Figure D-1 Sensitivity of cumulative tile flow, Q_{tc} , cumulative soil to groundwater percolation rate, G_c , and mean soil water
 1352 table saturated storage elevation, SS , to capillary fringe thickness, T_{CF} (a) capillary fringe drainable water, ϕ_c (b), soil hydraulic
 1353 conductivity, K (c), soil thickness, T_{SL} (d), sine function amplitude, A (e) and sine function intercept, B (f).

1354

1355 *D.1.1 Sensitivity to capillary fringe thickness*

1356 To gauge sensitivity to capillary fringe thickness T_{CF} , flow rates and the SS were analyzed for T_{CF}
1357 ranging 0 to 1600 mm. Figure D-1a indicates that as T_{CF} increases, both cumulative tile flow (Q_{tc})
1358 and mean soil ~~water tablesaturated storage~~ (SS) decline. The SS drop is sharper for T_{CF} beyond
1359 900 mm. Beyond this thickness, Q_{tc} stabilizes at a minimal value. A negative SS indicates its
1360 position below the tile pipe. G_c remains consistent despite T_{CF} variations.

1361

1362 *D.1.2 Sensitivity to capillary fringe drainable water*

1363 With rising φ_c both Q_{tc} and SS surge (Figure D-1b). As φ_c ascends from 0.005 to 0.45, Q_{tc} jumps
1364 from 1300 mm to 1900 mm and SS from -0.45 m to -0.25 m (Figure D-1b). G_c stays constant,
1365 irrespective of φ_c fluctuations.

1366

1367 *D.1.3 Sensitivity to soil hydraulic conductivity*

1368 Increasing soil hydraulic conductivity (K) from 0 to 10 mm hr⁻¹ leads to a surge in Q_{tc} and a drop
1369 in SS (Figure D-1c). However, adjusting K from 10 to 50 mm hr⁻¹ results in leveling off slopes for
1370 Q_{tc} and SS , especially when $K > 20$ mm hr⁻¹. Both metrics are acutely responsive to K when K is
1371 below 10 mm hr⁻¹ but become non-responsive beyond 20 mm hr⁻¹. G_c 's response to K remains
1372 neutral.

1373

1374 *D.1.4 Sensitivity to soil thickness*

1375 Similar to K , a rise in T_{SL} from 1500mm to 15000 mm cause Q_{tc} to rise and SS to decline (Figure
1376 D-1d). The most significant rate of change for both metrics occurs between 1500 to 5000 mm T_{SL} .
1377 Beyond 5000 mm, changes flatten. G_c shows no response to T_{SL} variations.

1378

1379 *D.1.5 Sensitivity to sine function amplitude*

1380 Increasing the sine function amplitude, A , from -0.03 to 0 mm hr⁻¹ pushes both Q_{tc} and SS increase
1381 and reach to their maximum at $A=0$ (Figure D-1e). But as A rises from 0 to 0.06 mm hr⁻¹, they both
1382 decline. In contrast, G_c descends to its lowest (400 mm) when A shifts from -0.03 to 0 and then
1383 increases to 900 mm as A hits 0.063 .

1384

1385 *D.1.6 Sensitivity to sine function intercept*

1386 Both Q_{tc} and SS ascend with the growth in sine function's intercept, B . Increasing B from -0.015
1387 to 0.005 mm hr⁻¹ sees G_c descend. During this B increase, Q_{tc} expands from 1100 to 2400 mm,
1388 while G_c shrinks from 1400 to 0 mm. It seems the sum of Q_{tc} and G_c might be constant. This
1389 suggests that water either drains through the tile pipe or percolates through the soil bottom.

1390 Q_{tc} , and SS appear sensitive to all six module parameters, but G_c only to A and B .

1391

1392 **D.2 Module parameter evaluation for new sites**

1393 As discussed in section 2.5, initial values for K , T_{CF} and φ_c can be determined by soil grain-size
1394 distribution. Parameters less explored in past research for new sites include the sine function's
1395 amplitude (A), intercept (B), and time delay (D_d).

1396

1397 *D.2.1 Evaluating sine function's A and B*

1398 If no percolation exists from the soil's bottom to groundwater and $G_{y,i}$ is zero, both A and B should
1399 be zero. However, if percolation or interactions between soil and groundwater occurs, A and B
1400 need calibration assessment. Before this, reasonable initial values and bounds must be set.
1401 From this study's findings, A and B should fall between the mean hourly difference of infiltration
1402 and observed tile flow rates. For instance, observed hourly rates for infiltration and tile flow at our
1403 site are 0.07 and 0.03 mm hr⁻¹. Thus, A 's and B 's initial values should range from -0.04 to 0.04
1404 mm hr⁻¹. Negative A and B values indicate outflow from soil to groundwater and vice versa. Initial
1405 values were set at 10% of the range limits: -0.004 for B and 0.004 for A . Eventually, B and A were
1406 adjusted to -0.005 and 0.025 mm hr⁻¹.

1407

1408 *D.2.2 Assessment of sine function's time delay*

1409 The sine function begins on the first Julian day. If its peak occurs around 91st Julian day (three
1410 months later), its minimum should be on the 274th day. If the peak comes later, say the 111th day,
1411 a 20-day delay is present. This delay should mirror in both function's minima and maxima. In this
1412 case the minimum would be on day 294. This delay aligns with the soil water table's peak annual
1413 fluctuations. When no observed fluctuations exist, the delay can be calibrated. A sensible initial
1414 delay can be ascertained by examining the study site's water table elevations, fitting a sine
1415 function, and noting the peak's Julian day annually.